

Robust Hybrid Learning With Expert Augmentation

Anonymous authors

Paper under double-blind review

Abstract

Hybrid modelling reduces the misspecification of expert models by combining them with machine learning (ML) components learned from data. Similarly to many ML algorithms, hybrid model performance guarantees are limited to the training distribution. Leveraging the insight that the expert model is usually valid even outside the training domain, we overcome this limitation by introducing a hybrid data augmentation strategy termed *expert augmentation*. Based on a probabilistic formalization of hybrid modelling, we demonstrate that expert augmentation, which can be incorporated into existing hybrid systems, improves generalization. We empirically validate the expert augmentation on three controlled experiments modelling dynamical systems with ordinary and partial differential equations. Finally, we assess the potential real-world applicability of expert augmentation on a dataset of a real double pendulum.

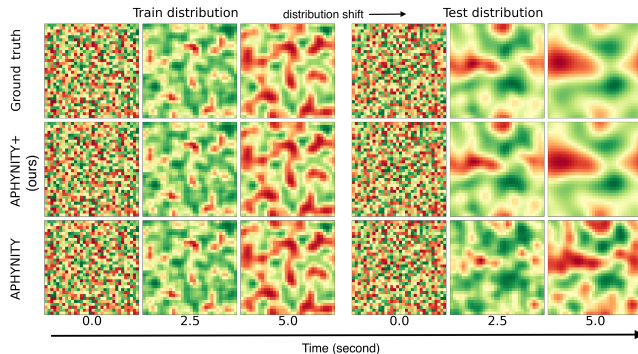


Figure 1: APHYNITY, an existing hybrid modelling strategy, is unable to predict accurately the dynamic of a 2D diffusion reaction for a shifted test distribution, although it predicts well configurations that follow the training distribution. APHYNITY+, the same model fine-tuned with our expert augmentation, generalizes to shifted distributions as expected from the validity of the underlying physics.

1 Introduction

Generalizing to unseen data is crucial to make a model applicable in the real world. When training and test data are independently and identically distributed (IID), we assess the model generalization on a held-out subset of the training data. Unfortunately, the training and test scenarios do not entirely overlap in practice. This observation has motivated many recent research efforts to focus on the robustness of ML models (Gulrajani & Lopez-Paz, 2020; Geirhos et al., 2020; Koh et al., 2021). Common strategies can be broadly grouped into two categories. The first class of methods aims to align properties of the model (e.g., invariance, equivariance or monotonicity) with expertise in the problem of interest (Cubuk et al., 2019; Mahmood et al., 2021; Keriven & Peyré, 2019; Silver et al., 2017). The second category is data-focused (Sagawa et al., 2019; Arjovsky et al., 2019; Krueger et al., 2021; Creager et al., 2021), and leverages variations present in the training data, e.g., some methods minimize the worst-case sub-group performance, to achieve robustness.

The data-oriented methods, which include Group-DRO (Sagawa et al., 2019) and Invariant Risk Minimization (Arjovsky et al., 2019, IRM), can be very appealing because they only require implicit specification

of invariances via domains or environments. However, these methods rely on variations in the training data, which may be insufficient when the problem is too complex, or the variations of interest are absent from the training set. On the other hand, methods based on domain-specific expertise do not suffer from such limitations. Embedding expertise into a model can be done via architectural inductive biases (LeCun et al., 1995; Xu et al., 2018), data augmentation (Cubuk et al., 2019), or a learning objective that enforces established symmetries of the problem (Cranmer et al., 2020). For example, simple data augmentation techniques combined with convolutions lead to excellent performance on natural image problems (Cubuk et al., 2019). Another natural approach to embedding expertise in ML models, and the one studied in this paper, is called hybrid learning. This framework combines an expert model (e.g., physics-motivated equations) with a learned component that improves the expert model so that the combination better fits real-world data. In hybrid learning, the expert model plays a central role and is supposed to provide a simple and well-grounded parametric description of the process considered. The expert model is often motivated by the underlying physics system’s. Hence, we will use the terms *expert* model and *physical* model interchangeably.

In recent works (Yin et al., 2021; Takeishi & Kalousis, 2021; Qian et al., 2021; Mehta et al., 2020; Lei & Mirams, 2021; Reichstein et al., 2019), hybrid learning demonstrated success in complementing partial physical models and improving the inference of the corresponding parameters. We observe that current hybrid learning algorithms are sub-optimal in the amortized inference setting – when we aim to build hybrid models that are valid for various test configurations. Contrary to the common belief that hybrid learning achieves better generalization than black box ML models, we argue and demonstrate that hybrid learning algorithms do not yet meet their promise regarding robustness in amortized settings. Although hybrid learning achieves strong performance on IID test distributions by exploiting the inductive bias of the expert models, their performance collapses when the test domain is not included in the training domain. This is unsatisfactory as the expert model is typically well-defined far outside the training distribution.

A test distribution not covered by the training data but for which an expert model exists often happens in the real world. For instance, Qian et al. (2021) apply hybrid learning to a pharmacological model describing the effect of a COVID-19 treatment for which only a limited quantity of real-world data is available. In this context, although the underlying biochemical dynamic of treatments is well modelled, data is often scarce and biased. Therefore, the hybrid model does not necessarily generalize to configurations that the pharmacological model well models if they are not part of the training set.

We introduce *expert augmentations* for training augmented hybrid models (AHMs), a procedure that extends the range of validity of hybrid models and improves generalization, as pictured by Figure 1. Our contribution is to first formalise the hybrid learning problem as: 1) Learning a probabilistic model partially defined by the expert model; 2) Performing inference over this probabilistic hybrid model. In this context, we show that hybrid learning is vulnerable to distribution shifts for which the expert model is well defined (see Figure 1, bottom row). Motivated by our analysis, we propose to fine-tune the hybrid model on an expert-augmented dataset that includes distribution shifts (see results of augmentation in Figure 1, middle row). These expert augmentations only rely on the hybrid model itself, leveraging that the expert model is also well-defined outside of the training distribution. Our experiments on various controlled problems demonstrate that AHMs improve the generalization capabilities of state-of-the-art hybrid learning algorithms on synthetic and real-world data in the amortize setting.

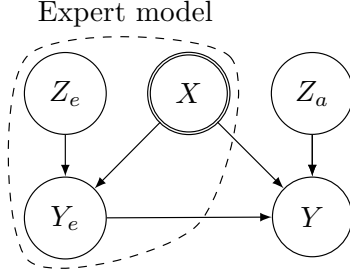


Figure 2: A hybrid probabilistic model which describes the relationship between a given input X and the output Y for a configuration of the system as defined by the latent variables Z_e and Z_a . The prescribed expert model defines the conditional density $p(y_e|z_e, x)$, where Y_e is an approximation of Y . Hybrid learning aims at learning the conditional distribution $p(y|z_a, y_e, x)$.

Algorithm 1 Expert augmented hybrid learning

```

1:  $\mathcal{D} := \{(x^{(i)}, y^{(i)})\}_{i=1}^N \in (\mathcal{X} \times \mathcal{Y})^N$   $\triangleright$  A training set
2:  $q_\psi(z_a, z_e|x, y)$   $\triangleright$  A parametric encoder
3:  $p(y_e|x, z_e)$   $\triangleright$  An expert model
4:  $p_\theta(y|x, y_e, z_a)$   $\triangleright$  A parametric interaction model
5:  $l(x, y, \theta, \psi)$   $\triangleright$  A hybrid learning objective function
6:  $p_+(z_e)$   $\triangleright$  A prior distribution on  $z_e$  that covers both train and test scenarios
7: procedure TRAINING
8:    $\psi^*, \theta^* \leftarrow \arg \min_{\psi, \theta} \mathbb{E}_{(x, y) \sim \mathcal{D}} [l(x, y, \theta, \psi)]$ 
9:    $\theta^*$  is frozen.
10:   $\mathcal{D}^+ \leftarrow \text{GENERATEAUGMENTEDSET}$ 
11:   $\mathcal{D} \leftarrow \mathcal{D} \cup \mathcal{D}^+$ 
12:  Finetuning the encoder on the augmented training set:
13:   $\psi^* \leftarrow \arg \min_{\psi} \mathbb{E}_{(x, y) \sim \mathcal{D}} [l(x, y, \theta^*, \psi)]$ 
14:     $- \mathbb{E}_{(x, y, z_e) \sim \mathcal{D}^+} [\log q_\psi(z_e|x, y)]$ 
15: end procedure
16: procedure GENERATEAUGMENTEDSET
17:   $\mathcal{D}^+ \leftarrow \{\}$ 
18:  for each  $(x_o, y_o) \in \mathcal{D}$  do
19:     $z_a \sim q_{\psi^*}(z_a, z_e|x_o, y_o)$ 
20:     $z_e \sim p_+(z_e)$ 
21:     $y_e \sim p(y_e|x_o, z_e)$ 
22:     $y \sim p_{\theta^*}(y|x_o, y_e, z_a)$ 
23:     $\mathcal{D}^+ \leftarrow \mathcal{D}^+ \cup \{(x_o, y, z_e)\}$ 
24:  end for
25:  return  $\mathcal{D}^+$ 
26: end procedure

```

2 Hybrid learning

In order to show that our proposed expert augmentations lead to robust models, we first formalize hybrid learning with the probabilistic model depicted in Figure 2. In this Bayesian network, capital letters denote random variables (e.g., Y) and, in the following, we will use calligraphic letters for the domain of the corresponding realization (e.g., $y \in \mathcal{Y}$). In our formalism, the expert model is a conditional density $p(y_e|x, z_e)$ that describes the distribution of the *expert* response Y_e to an input x together with a parametric description of the system z_e , denoting expert or physical parameters. We augment the expert model with the *interaction model* which is a conditional distribution $p(y|x, y_e, z_a)$ that describes the distribution of the observation Y given the input x , the expert model response y_e , and a parametric description of the interaction model z_a .

Our goal is to create a robust predictive model $p(y|x, (x_o, y_o))$ of the random variable Y , given the input x together with independent observations (x_o, y_o) of the same system, where the subscript o denotes an observed quantity. As a concrete example, we consider predicting the evolution of a damped pendulum (described in Section 4.1) given its initial angle and speed ($x = [\theta, \dot{\theta}]$) and a sequence of observations of the same pendulum. The expert model we assume is able to describe a frictionless pendulum whose dynamic is only characterized by one parameter $z_e := \omega_0$, denoting its fundamental frequency. The expert model is misspecified. It does not model the friction with a second parameter $z_a := \alpha$, the damping factor. In this problem, (x_o, y_o) and (x, y) are IID realization of the same pendulum which corresponds, in general terms, to samples from $p(x, y|z_a, z_e)$ for some fixed but unknown values of z_a and z_e . The expert variables z_e (e.g., ω_0) together with z_a (e.g., α) should accurately describe the system that produces Y (e.g., the evolution of

the pendulum’s angle and speed along time) from X (e.g., the initial pendulum’s state). In our setting we assume that we are given a pair (x_o, y_o) (e.g., past observations) from which we can accurately infer the state of the system (z_a, z_e) as described by the interaction and expert models, and then predict the distribution of Y for a given input x (e.g., forecasting future observations) to the same system. Provided all probability distributions in Figure 2 are known, the Bayes optimal hybrid predictor p_B is

$$p_B(y|x, (x_o, y_o)) = \mathbb{E}_{p(z_a, z_e|(x_o, y_o))} [p(y|x, z_a, z_e)], \quad (2)$$

as shown in Appendix E. In the amortized setting, we aim to learn a model of both the predictive model $p(y|x, z_a, z_e)$ and of the posterior over the parameters $p(z_a, z_e|(x_o, y_o))$. We will see that existing hybrid learning algorithms neglect the importance of building a robust encoder $p(z_a, z_e|(x_o, y_o))$ to make predictions in out-of-distribution (OOD) settings. We expect that the interaction between z_e and y is essentially defined by the expert model thus it should be possible, and preferable, to learn an predictive model of Y whose performance guarantees are as independent as possible from the training distribution of the expert variables z_e . Indeed, the range of validity of the expert model might be broader then the observed training configurations. However, we demonstrate below that existing algorithms’ performance collapses when the distribution of z_e shifts. The expert augmentation introduced in this paper improves the robustness of hybrid models to such shifts.

2.1 Hybrid generative modelling

We consider expert models that are deterministic; that is, for which $p_\theta(y_e|x, z_e)$ is a Dirac distribution. The expert model describes the system as a function $f_e : \mathcal{X} \times \mathcal{Z}_e \rightarrow \mathcal{Y}_e$ that computes the response y_e to an input x , parameterized by expert variables z_e . The goal of hybrid modelling is to augment the expert model with a learned component from data as depicted in Figure 2. Formally, given a dataset $\mathcal{D} = \{(x^{(i)}, y^{(i)})\}_{i=1}^N$ of N IID samples, we aim to learn the interaction model $p_\theta(y|x, y_e, z_a)$ that fits the data well but is close to the expert model. For example, we could define closeness via a small L2-distance between expert and hybrid outputs or via a small Kullback-Leibler (KL) divergence between the marginal distributions of Y and Y_e .

Learning a model that is close to the expert model and fits the training data well is a hard problem. However, the APHYNITY algorithm (Yin et al., 2021) and the Hybrid-VAE (Takeishi & Kalousis, 2021, HVAE) are two recent approaches that offer promising solutions to this problem. We now briefly describe how these methods approximate the Bayes optimal predictor of Equation (2). Our augmentation strategy is compatible (and effective) with both approaches.

APHYNITY. Yin et al. (2021) formulate hybrid learning in a context where the expert model is an ordinary differential equation (ODE). They consider an additive hybrid model that should perfectly fit the data, which is equivalent to assuming the conditional distribution $p_\theta(y|x, y_e, z_a)$ is a Dirac distribution. Formally, they solve the optimization problem

$$\begin{aligned} \min_{z_e, F_a} \|F_a\| \quad \text{s.t.} \quad & \forall (x, y) \in \mathcal{D}, \forall t, \frac{dy_t}{dt} = F_e(y_t) + F_a(y_t) \\ & \text{with } y_0 := x, \end{aligned} \quad (3)$$

where $\|\cdot\|$ is a norm operator on the function space, $F_a : \mathcal{Y}_t \times \mathcal{Z}_a \rightarrow \mathcal{Y}_t$ is a learned function, $F_e : \mathcal{Y}_t \times \mathcal{Z}_e \rightarrow \mathcal{Y}_t$ defines the expert model and \mathcal{D} is a dataset of initial states $x := y_0$ and sequences $y \in \mathcal{Y} := (\mathcal{Y}_t)^k$, where k is the number of observed timesteps. APHYNITY solves this problem with Lagrangian optimization and Neural ODEs (Chen et al., 2018) to compute derivatives. In the context of ODEs, the random variable X is the initial state of the system at t_0 and Y is the observed sequence of k states between t_0 and t_1 .

This formulation only considers learning a missing dynamic for one realization of the system described by Figure 2, for a single z_a and z_e . However, we are interested in learning a hybrid model that works for the full set of systems described by Figure 2. As suggested in Yin et al. (2021), we use an encoder network $g_\psi(\cdot, \cdot) : \mathcal{X} \times \mathcal{Y} \rightarrow \mathcal{Z}_a \times \mathcal{Z}_e$ that corresponds to a Dirac distribution located at g_ψ as the approximate posterior $q_\psi(z_a, z_e|x, y)$. The interaction model is a product of Dirac distributions whose locations correspond to the

solution of the ODE

$$\frac{dy_t}{dt} = F_e(y_t, z_e) + F_a(y_t, z_a; \theta), \quad y_0 := x. \quad (4)$$

Hence the corresponding approximate Bayes predictor replaces the parameters (z_a, z_e) in Equation (4) with the prediction of g_ψ and predicts a product of Dirac distributions.

Hybrid-VAE (HVAE). In contrast to APHYNITY, the hybrid-VAE proposed by Takeishi & Kalousis (2021) is not limited to additive interactions between the expert model and the ML model, nor to ODEs. Instead, their goal is to learn the generative model described by Figure 2. They achieve this with a variational auto-encoder (VAE) where the decoder specifically follows Figure 2. Similarly to the amortized APHYNITY model, the encoder $g_\psi(x, y)$ predicts a posterior distribution over z_a and z_e , and the model is trained with the classical Evidence Lower Bound on the likelihood (ELBO). Takeishi & Kalousis (2021) observe that relying only on an architectural inductive bias and maximum likelihood training is not enough to ground the generative model to the expert equations. They propose to add three regularizers R_{PPC} , $R_{DA,1}$, and $R_{DA,2}$ that encourage the generative model to rely on the expert model. The final objective is

$$\max_{\theta, \psi} \mathbb{E}_{\mathcal{D}} [\text{ELBO}((x, y); \psi, \theta)] + \alpha R_{PPC} + \beta R_{DA,1} + \gamma R_{DA,2}. \quad (5)$$

The first regularizer, R_{PPC} , encourages the marginal distribution of samples generated by the complete model to be close to the marginal distribution that would be only generated by the physical model. The two other regularizers specifically require the encoder network for z_e to be made of two sub-networks. The first network filters the observations to keep only what can be generated by the expert model alone, and the second should map the filtered observations to the posterior distribution over z_e . $R_{DA,1}$ penalizes the objective if the observations generated by the expert model are not close to the filtered observations. Finally, $R_{DA,2}$ relies on data augmentation with the expert model to enforce that the second sub-network correctly identifies the expert variables z_e when the observations are correctly filtered. We refer the reader to Appendix B and Takeishi & Kalousis (2021) for more details on HVAE. For HVAE, the approximate predictor takes the form described by Equation (2) where $p(z_a, z_e | (x_o, y_o))$ is approximated by the encoder $q_\psi(z_a, z_e | x, y)$ and $p(y | x, z_a, z_e)$ by the learned hybrid generative model.

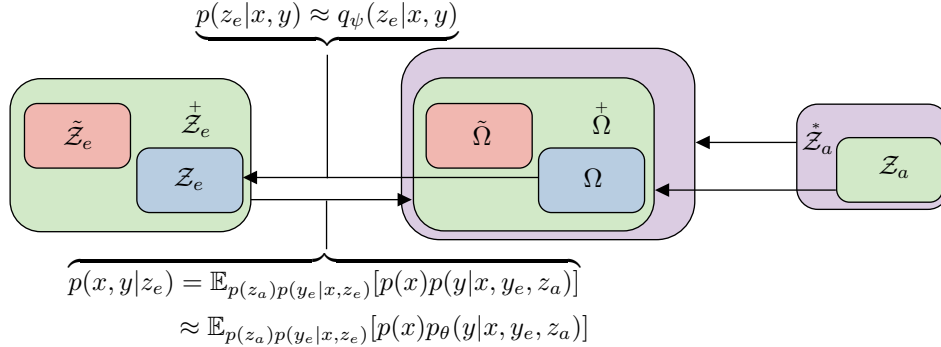


Figure 3: Visualization of the distribution shifts considered in this work. The train support Ω of (x, y) results from $(z_a, z_e) \in \mathcal{Z}_a \times \mathcal{Z}_e$. The test supports (in red) are denoted with a tilde symbols as $\tilde{\mathcal{Z}}_e$ for z_e and $\tilde{\Omega}$ for (x, y) . The augmented support $\tilde{\Omega}^+$ (in green) includes both train and test scenarios and corresponds to $(z_a, z_e) \in \mathcal{Z}_a \times \mathcal{Z}_e^+$. The outer violet domain that includes $\tilde{\Omega}^+$ depicts one of our experiment in which the domain of z_a is also shifted. Hybrid modelling algorithms alone may learn a mapping $p_\theta : \mathcal{Z}_e^+ \rightarrow \tilde{\Omega}^+$ but augmentation is necessary to learn the inverse mapping $q_\psi : \tilde{\Omega}^+ \rightarrow \mathcal{Z}_e^+$.

3 Robust hybrid learning

We now formalize our definition of out of distribution (OOD) and robustness. In general, a test scenario is OOD if the joint test distribution $\tilde{p}(x, y)$ is different from the training distribution $p(x, y)$, that is $d(\tilde{p}, p) > 0$

for any properly defined divergence or distance d . In the following, we reduce our discussion to a sub-class of distribution shifts for which the marginal train and test distributions over z_e may be different, $d(p(z_e), \tilde{p}(z_e)) > 0$, but the marginals of z_a and x are constant. As a consequence, the joint distribution of (x, y) pairs is also shifted. Formally, the training and test distributions are respectively defined as

$$\begin{aligned} p(x, y) &:= \mathbb{E}_{p(z_e)p(z_a)p(y_e|x, z_e)} [p(x)p(y|x, y_e, z_a)], \\ \tilde{p}(x, y) &:= \mathbb{E}_{\tilde{p}(z_e)p(z_a)p(y_e|x, z_e)} [p(x)p(y|x, y_e, z_a)]. \end{aligned}$$

In this context, we demonstrate, theoretically and empirically, that classical hybrid models fail. To address this failure, we introduce *augmented hybrid models* and show that, under some assumptions, they achieve optimal performance on both the train and test distributions.

Our goal is to learn a predictive model

$$p_{\theta, \psi}(y|x, (x_o, y_o)) = \mathbb{E}_{q_{\psi}(z_a, z_e|x_o, y_o)} [p_{\theta}(y|x, y_e, z_a)]_{p(y_e|x, z_e)}$$

that is *exact* on both the train and test domains when they follow the aforementioned training and testing distribution shifts. We say that a learned predictive model $\hat{p}(a|b)$ is \mathcal{E} -*exact*, or *exact* on the sample space \mathcal{E} , if $\hat{p}(a|b) = p(a|b) \quad \forall (a, b) \in \mathcal{E}$. Here we qualify a predictive model as *robust* to a test scenario if its *exactness* on the training domain is sufficient to ensure exactness on the test domain.

We now define an augmented distribution $\overset{+}{p}(z_e)$ over the expert variables whose support $\overset{+}{Z}_e$ includes the joint support $Z_e \cup \tilde{Z}_e$ between the train and test distribution of the physical parameters. As depicted in Figure 3, we denote the corresponding support over the observation space $\mathcal{X} \times \mathcal{Y}$ as $\overset{+}{\Omega}$ for the augmented distribution, Ω for the training distribution, and $\tilde{\Omega}$ for the test distribution. In this context, and with **A1**, we may demonstrate that even under perfect learning, classical hybrid learning algorithms do not produce an $\tilde{\Omega}$ -*exact* predictor while our augmentation strategy does.

Assumption 1 (A1): *Hybrid modelling learns an interaction model $p_{\theta}(y|y_e, x, z_a)$ that is $\overset{+}{\Omega}$ -exact.*

Although strong, **A1** is consistent with the recent literature on hybrid modelling, which assumes that the expert model $p(y_e|x, z_e)$ is an accurate description of the system, thereby the interaction model $p_{\theta}(y|y_e, x, z_a)$ should not be overly complex. As an example, we consider an additive interaction model in our experiments for which extrapolation to unseen y_e holds if the additive assumption is correct. That said, we still notice that the exactness of the interaction model p_{θ} on the augmented support $\overset{+}{\Omega}$ is insufficient to prove that the predictive model $p_{\theta, \psi}$ is $\overset{+}{\Omega}$ -*exact*. Indeed, the encoder q_{ψ} is only trained on the training data and cannot rely on a strong inductive bias in contrast to p_{θ} . Thus, even if the encoder is exact on the training distribution, the corresponding predictive model is not $\overset{+}{\Omega}$ -*exact*. While the decoder’s performance are not limited to the training scenarios thanks to the broader validity of the expert model, the encoder does not generalize to unseen settings as it is purely data-driven.

3.1 Expert augmentation

We propose a data augmentation strategy to improve the robustness of hybrid models to unseen test scenarios. Once trained, the hybrid model is composed of an encoder q_{ψ} and an interaction model p_{θ} that are respectively Ω - and $\overset{+}{\Omega}$ -*exact*. We may create a new training distribution with a support over $\overset{+}{\Omega}$ by sampling physical parameters z_e from a distribution that covers $\overset{+}{Z}_e$. Then, we train the encoder q_{ψ} on the augmented domain $\overset{+}{\Omega}$, under perfect training the predictive model $p_{\theta, \psi}(y|x, (x_o, y_o))$ is $\overset{+}{\Omega}$ -*exact*, hence exact on both train and test domains. The expert augmentation is formally described in algo:augmentation.

Our learning strategy is grounded in existing hybrid modelling algorithms, and here, we focus on APHYNITY and HVAE. We first train an encoder q_{ψ} and a decoder p_{θ} with a hybrid learning algorithm. Together with experts we then decide on a realistic distribution $\overset{+}{p}(z_e)$ and create a new dataset $\overset{+}{\mathcal{D}} := \{(z_e, x_i, y_i)\}_{i=1}^{\overset{+}{N}}$ by sampling from the hybrid generative model defined by Figure 2 and the interaction model p_{θ} . A notable

difference between the augmented training set $\bar{\mathcal{D}}^+$ and the original training set \mathcal{D} is that the former contains ground truth values for the expert’s variables z_e . As we assume that the interaction model is $\bar{\Omega}^+$ -exact, we freeze it and only fine-tune the encoder q_ψ on $\bar{\mathcal{D}}^+$. We use a combination of the loss function ℓ of the original algorithm (e.g., Equation (5) for HVAE, and the Lagrangian of Equation (3) for APHYNITY) and a supervision on the latent variable objective to learn a decoder that solves

$$\begin{aligned}\psi^* &= \arg \min_{\psi} \mathbb{E}_{p(z_e)p(z_a)p(x)p(y|x,z_e,z_a)} [\ell(x,y;\theta,\psi) - \log q_\psi(z_e|x,y)], \\ &\approx \arg \min_{\psi} \frac{1}{N} \sum_{(z_e,x,y) \in \bar{\mathcal{D}}^+} \ell(x,y;\theta,\psi) - \log q_\psi(z_e|x,y).\end{aligned}\tag{6}$$

In our experiments we chose a Gaussian model for the posterior, which is equivalent to a mean squared error (MSE) loss on the physical parameters. We provide a detailed description of the expert augmentation scheme in Appendix A. In principle, we could also remove the regularizers, the norm of f_a for APHYNITY or αR_{PPC} , $R_{DA,1}$, and $R_{DA,2}$ for the Hybrid-VAE, from the loss function l as Equation (6) only aims to improve the encoder whereas these terms mainly aim to regularize the interaction model. However, in practice, we have observed that this does not matter.

As a side note, we would like to emphasize the difference between the data augmentation proposed in this paper and the one from Takeishi & Kalousis (2021). While HVAE also requires to sample new physical parameters z_e , it is only to ensure that a sub-part of the encoder is able to infer correctly z_e given y_e . This augmentation does not contribute robustness to distribution shifts on y in contrast to ours.

4 Experiments

We assess the benefits of expert augmentation on three synthetic problems and one real-world experiment that are described by the ODE

$$\frac{dy_t}{dt} = F_e(y_t; z_e) + F_a(y_t; z_a),\tag{7}$$

where $F_e : \mathcal{Y}_t \times \mathcal{Z}_e \rightarrow \mathcal{Y}_t$ is the expert model and $F_a : \mathcal{Y}_t \times \mathcal{Z}_a \rightarrow \mathcal{Y}_t$ complements it. In our notation X is the initial state y_0 and the response Y is the sequence of states $y_{1:t_1} := [y_{i\Delta t}]_{i=1}^{t_1/\Delta t}$. For all experiments we train the models to maximize $p_{\theta,\psi}(y = y_{1:t_1} | x = y_0)$ on the training data. We validate and test the models on the predictive distribution $p(y = y_{1:t_2} | x = y_0, x_o = y_0, y_o = y_{1:t_1})$, where $t_2 > t_1$ assesses the generalization over time. A brief description of the different problems is provided below.

4.1 Synthetic experiments

The damped pendulum is often used as an example in the hybrid modelling literature (Yin et al., 2021; Takeishi & Kalousis, 2021). The system’s state at time t is $y_t = [\theta_t \ \dot{\theta}_t]^T$, where θ_t is the angle of the pendulum at time t and $\dot{\theta}_t$ its angular speed. The evolution of the state over time is described by Equation (7), where $z_e := \omega$, $z_a := \alpha$ and

$$F_e := [\dot{\theta} \ -\omega_0^2 \sin \theta]^T \quad \text{and} \quad F_a := [0 \ -\alpha \dot{\theta}]^T.\tag{8}$$

The corresponding systems are defined by the damping factor α and ω_0 , the fundamental frequency of the pendulum.

The RLC series circuits are electrical circuits made of 3 electrical components that may model a large range of transfer functions. A schematic of such circuit is shown in Figure 10. These models are often used in biology (e.g., the Hodgkin-Huxley class of models (Hodgkin & Huxley, 1952), in photoplethysmography (Crabtree & Smith, 2003)) and in electrical engineering to model the dynamics of various systems. The system’s state at time t is $y_t = [U_t \ I_t]^T$, where U_t is the voltage over the capacitor and I_t the current in the circuit. The evolution of the state over time is described by Equation (7), where $z_e := \{L, C\}$, $z_a = \{R\}$ and

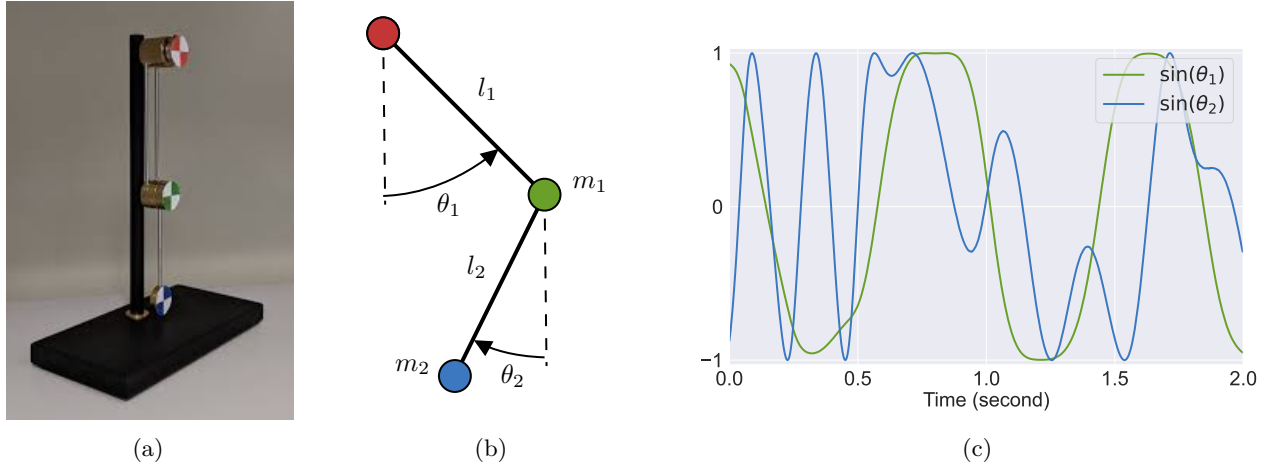


Figure 4: The double pendulum setup. (a) A photograph of the double pendulum at rest, reproduced from Asseman et al. (2018). (b) A simplified sketch of the setup. (c) An example of the time series extracted from the videos of the double pendulum.

$$F_e := \left[\frac{I_t}{L} \right] \quad \text{and} \quad F_a := \left[\begin{array}{c} 0 \\ -\frac{R}{C} I_t \end{array} \right]. \quad (9)$$

The dynamics described by the RLC circuit is more diverse than for the pendulum and the system can be hard to identify. This system is characterised by the resistance R , capacitance C , and inductance L , provided V_t is known.

The 2D reaction diffusion was used by Yin et al. (2021) to assess the quality of APHYNITY. It is a 2D FitzHugh-Nagumo on a 32×32 grid. The system’s state at time t is a $2 \times 32 \times 32$ array $y_t = [u_t \ v_t]^T$. The evolution of the state over time is described by Equation (7), where $z_e := \{a, b\}$, $z_a = \{k\}$ and

$$F_e := \left[\begin{array}{c} a \Delta u_t \\ b \Delta v_t \end{array} \right] \quad \text{and} \quad F_a := \left[\begin{array}{c} R_u(u_t, v_t; k) \\ R_v(u_t, v_t) \end{array} \right], \quad (10)$$

where Δ is the Laplace operator, the local reaction terms are $R_u(u, v; k) = u - u^3 - k - v$ and $R_v(u, v) = u - v$. This model is interesting to study as it considers a state space for which neural architectures may have a real advantage compared to other ML models. In particular, convolutional neural networks are effective for processing signals with spacial and/or temporal correlation.

In these experiments we analyze the effect of our data augmentation strategy on APHYNITY and HVAE. All models explicitly use the assumption that the interaction model follows the structure of Equation (7). For each problem the validation and test sets are respectively IID and OOD with respect to the training distribution. The best models are always selected based on validation performance, that is with samples from Ω . We provide additional details on the different expert models, dataset creation, and neural networks architectures in Appendix C.

4.2 A real world dataset - the double pendulum

We next validate the benefit of the expert augmentation in a controlled real-world setting. The dataset of a double pendulum introduced by Asseman et al. (2018) contains 21 videos of the pendulum shown in Figure 4a. Each run lasts approximately 40 seconds and is recorded at 400Hz. We can extract the position of the pendulum limbs from each frame with elementary computer-vision tools. Each recording starts from different initial conditions, leading to many states of this chaotic system. For illustration, we showcase the evolution of the arms’ angles over time in Figure 4c.

We sketch a simplified representation of the double pendulum in Figure 4b. Its state is a four-dimensional vector $y_t = [\theta_1(t) \ \theta_2(t) \ \dot{\theta}_1(t) \ \dot{\theta}_2(t)]^T$, containing the position and speed of both masses. We can derive

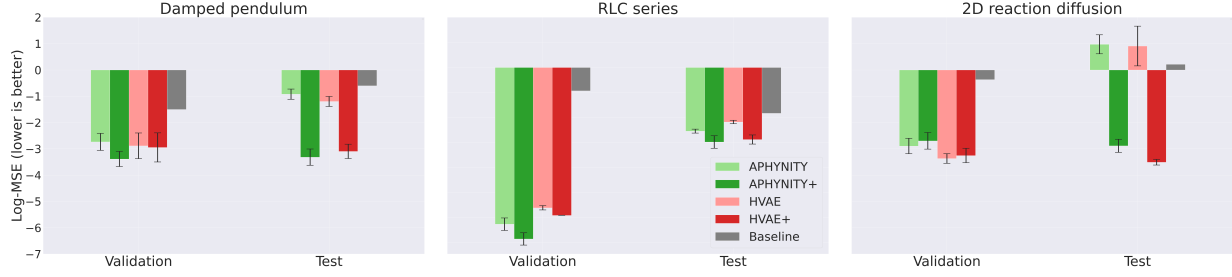


Figure 5: The average log-MSEs over 10 runs for three synthetic problems on the validation and test sets. We compare HVAE (in red) and APHYNITY (in green), in light colours, to their expert augmented versions HVAE+ and APHYNITY+, in darker colours. *On the test sets, AHMs outperform the original models, and by a large margin on the pendulum and diffusion problems. Moreover, augmentation conserves the relatively good performance on the validation set (IID w.r.t. the training set).*

(e.g., (Stachowiak & Okada, 2006)) the kinetics of the frictionless pendulum from first-principle physics,

$$\ddot{\theta}_1 = \frac{-g(2m_1 + m_2) \sin \theta_1 - m_2 g \sin(\theta_1 - 2\theta_2) - 2 \sin(\theta_1 - \theta_2) m_2 (\dot{\theta}_2^2 l_2 + \dot{\theta}_1^2 l_1 \cos(\theta_1 - \theta_2))}{l_1(2m_1 + m_2 - m_2 \cos(2\theta_1 - 2\theta_2))}, \quad (11)$$

$$\ddot{\theta}_2 = \frac{2 \sin(\theta_1 - \theta_2) (\dot{\theta}_1^2 l_1 (m_1 + m_2) + g(m_1 + m_2) \cos \theta_1 + \dot{\theta}_2^2 l_2 m_2 \cos(\theta_1 - \theta_2))}{l_2(2m_1 + m_2 - m_2 \cos(2\theta_1 - 2\theta_2))}. \quad (12)$$

This ODE is a suitable expert model candidate for a real-world double pendulum.

We assume that $m_1 = m_2$. Therefore the effect of masses reduces to constant values in the expert ODE. The length of the two arms are known, $l_1 = 91mm$ and $l_2 = 70mm$. The total energy of the double pendulum decreases over time in all videos, which lets us speculate about frictions, not explained by the expert model. In addition, the expert model does not consider potential vibrations or errors in extracting the arms’ positions. Hybrid learning has the potential to correct these mispecifications automatically. In comparison, the characterisation of the frictions from first-principle physics is challenging and is still a research subject (Aghili, 2020).

Similarly to the damped pendulum, we consider the initial angular positions, $\theta_1(t=0)$ and $\theta_2(t=0)$, known. The encoder must predict the initial angular speeds $z_e := \{\dot{\theta}_1(t=0), \dot{\theta}_2(t=0)\}$ which are the only free parameters of the expert model. The encoder only observes θ_1 between $t=0ms$ to $t=10ms$ and θ_2 between $t=5ms$ to $t=10ms$ which makes the estimation of z_e complicated. Then we predict the angular positions between $t=0$ and $t=20ms$ given $\theta_1(t=0)$ and $\theta_2(t=0)$ and the estimation of $z_e := \{\dot{\theta}_1(t=0), \dot{\theta}_2(t=0)\}$ via the hybrid decoder.

We create a dataset with many initial conditions by splitting the videos into consecutive chunks of 20 frames sub-sampled at 100Hz, i.e., 200ms of video. We construct a distribution shift, as shown in Figure 11 from Appendix C.5, over the expert variables z_e by splitting each 40 seconds sequence into three parts. The training set only contains chunks from the last 16 seconds of each run. It corresponds to configurations with smaller energy and, thus, slower angular speeds than the test set, which only contains frames from the first 12 seconds. The validation set contains the remaining 12 seconds of frames in the middle.

4.3 Results

Performance gain from augmentation. *This experiment demonstrates that HVAE and APHYNITY are not robust to OOD test scenarios in opposition to the corresponding AHMs, as shown in Figure 1 for the 2D diffusion problem and in Appendix D for the two other problems. We emphasize that our intention is not to declare a winner between HVAE and APHYNITY. Indeed, both algorithms have already demonstrated performance superior to black box ML models. Hence, we only report a very simple baseline that is the mean value of the signals. We want to compare performance in OOD settings and empirically validate the benefit of AHMs. We compare the predictive performance in Figure 5 (see Table 1 for the raw numbers). Although*

classical hybrid learning strategies do very well on the IID validation set, they exhibit poor generalization on OOD test sets for all three problems. We also observe some disparity between APHYNITY and HVAE. In addition to different learning strategies, this is probably due to differences in the networks’ architectures as they were respectively inspired from the corresponding pendulum experiment in each paper. However, even if one method may outperform the other for some problems, they both benefit from our augmentation strategy (APHYNITY+, HVAE+). Overall, the effect of augmentation goes up to dividing the test error by a factor of $e^{4.6} \approx 100$ in some cases.

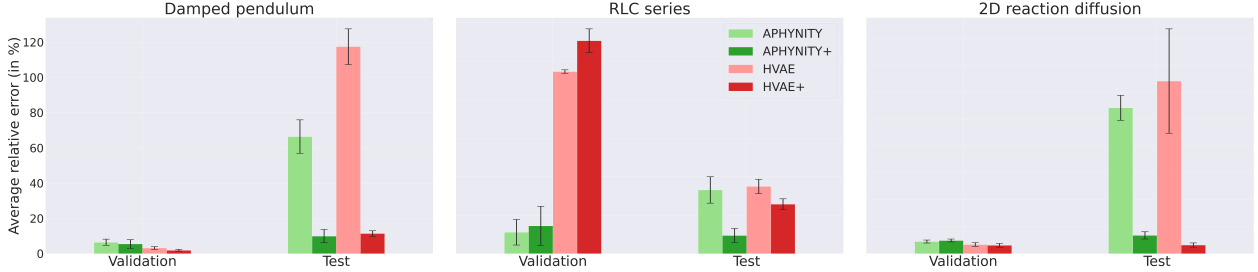


Figure 6: Comparison of mean relative precision (in %, \pm indicates one standard deviation) over 10 runs of predicted physical parameters of different hybrid modelling strategies in validation and OOD test settings. Augmented versions are denoted with a +. While the accuracy of APHYNITY and HVAE is good on the validation set, it collapses on the OOD test set. On the opposite, the augmented versions perform well on both validation and test sets.

Stability for non-exact models. The empirical results from Figure 5 are very important as they show that even when the decoder is not Ω -exact (and hence not Ω^+ -exact), augmentation may still work. In particular, Figure 6 shows that the encoder does not predict the physical parameters perfectly. This indicates that the encoder is not Ω -exact and neither should be the decoder. This plot shows the relative error on the physical parameters computed as $\sum_{i=1}^k \frac{1}{k} \left| \frac{z_e^i - \mu_\theta^i}{z_e^i} \right|$, where μ_θ^i is the estimated most likely value of the i^{th} component of the physical parameters. We first notice that APHYNITY and HVAE perform differently and their performance depends on the specific problem. While APHYNITY accurately estimates the physical parameters on the IID validation set for the 3 problems, HVAE’s performance are mixed on the RLC problem as it makes prediction that are around 120% away from the nominal parameter value on average whereas APHYNITY reduces this error to 6%. Interestingly, we observe that the proposed augmentation strategies improve the encoder such that it accurately estimates the physical parameters also on the OOD test set even for HVAE on the RLC problem. This confirms that the augmentation strategy is helpful even when the hybrid model is not Ω -exact. As a conclusion, augmented hybrid learning outperforms classical hybrid learning both on the predictive accuracy and at inferring the expert variables.

Effect of out of expertise shift. This experiment supports that our augmentation strategy may remain beneficial even when the train and test supports of z_a are not identical. This scenario corresponds to samples (x, y) generated by $(z_a, z_e) \in (\tilde{\mathcal{Z}}_a \setminus \mathcal{Z}_a) \times \tilde{\mathcal{Z}}_e$ depicted by the violet domains in Figure 3. In Figure 7 we observe the log-MSE of augmented and non-augmented hybrid models trained for $(z_a, z_e) \in \mathcal{Z}_a \times \mathcal{Z}_e$ on test data that are generated with $(z_a, z_e) \in \tilde{\mathcal{Z}}_a \times \tilde{\mathcal{Z}}_e$. For the pendulum, the support over $z_a = \alpha$ is $[0, 0.3]$ in train and $[0.3, 0.6]$ in test; For the 2D reaction diffusion, $z_a = k$ is $[0.003, 0.005]$ in train and $[0.005, 0.008]$ in test. We observe that augmented models outperform the original models by a large margin. These results suggest that augmentation could be very valuable in practice, even when the distribution shift is also caused by non expert variables. However, if the shift on z_a becomes the dominant effect, augmented models also eventually becomes vulnerable to shifts on z_e as demonstrated by supplementary experiments in Appendix C.

Real-world double pendulum. In Figure 9, we compare the empirical performance of APHYNITY(+) and HVAE(+) with two baselines: 1) *Expert only*: the ODE of a friction-less double pendulum, 2) *ML only*: an agnostic neural ODE. We conclude the potential effectiveness of expert augmentation for real-world settings from this experiment. We observe in Figure 9a that the augmentation improves the validation and test predictive performance by a non-negligible margin, as confirmed visually by Figure 8. In addition, the

augmentation improves the estimation of the expert parameters by up to a factor of two for APHYNITY in the OOD test scenarios, as shown in Figure 9b. In order to achieve these results, we finetune the encoder on expert augmentations with $\theta_1 \sim \mathcal{U}[-15, 15]$ and $\theta_2 \sim \mathcal{U}[-30, 30]$.

We have observed that optimizing the HVAE on the double pendulum data eventually becomes numerically unstable along training. It is why we did not manage to obtain HVAE’s performance on par with APHYNITY and the ML only baseline. In consequence, the expert augmentation is also unstable if it relies on the best model. We circumvent these numerical issues by applying the expert augmentation to an earlier version of the HVAE model. The expert augmented model outperforms the best HVAE model on predicting the trajectory as seen in Figure 9a. Finally, we study the effect of applying the expert augmentation at various stages during training for APHYNITY in Appendix D.4. We observe that expert augmentation may reduce the gap between the train/validation/test performance on the double pendulum even when the interaction model is not fully trained. This result hints again that expert augmentation can help even when the interaction model is not learned perfectly.

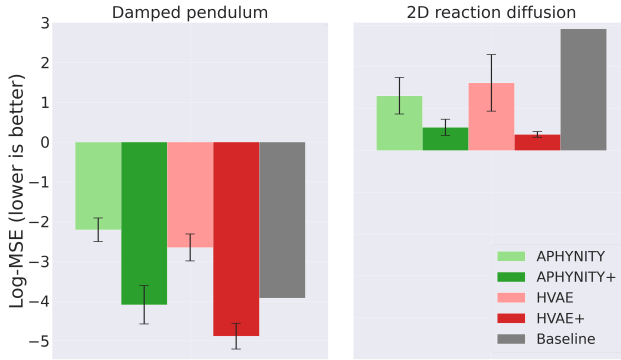


Figure 7: The average log-MSEs over 10 runs for the *damped pendulum* and *2D reaction diffusion* problems on a test distribution for which z_a , in addition to z_e , is also shifted. *AHM achieves better performance than standard algorithms even when the test distribution support z_a differs from the training.*

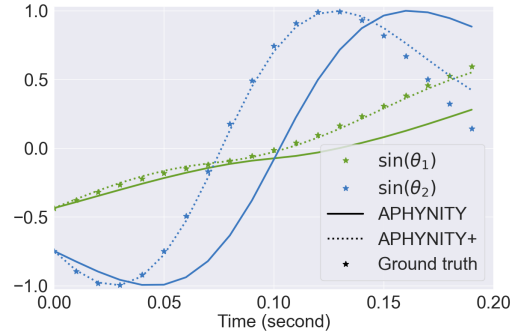


Figure 8: A cherry-picked example of the predicted angular positions of the double pendulum. *We observe that the proposed expert augmentation allows the hybrid model to predict more accurately the state of the double pendulum in the future than the non-augmented hybrid model.*

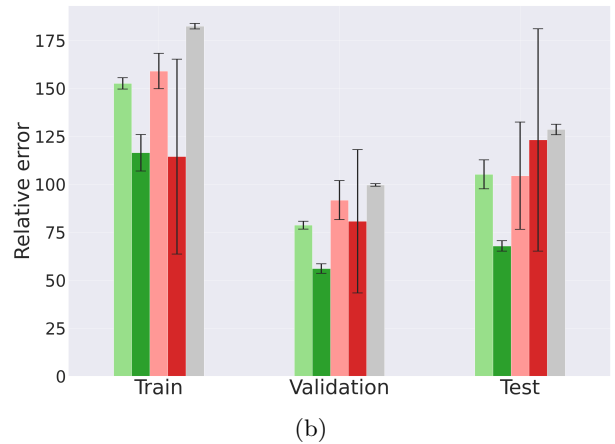


Figure 9: The results of the double pendulum experiment. (a) The average log-MSEs over three experiments. The baselines rely either only on the expert ODE or a neural ODE to predict the pendulum’s state. *The proposed expert augmentation slightly reduces the predictive performance on the training set for APHYNITY but increases the generalisation capabilities of both APHYNITY and the HVAE. APHYNITY+ outperforms the baselines on all sets.* (b) The average relative errors on the initial angular speeds over three runs. *The proposed expert augmentation improves the accuracy of the physical parameters estimation both in the IID and OOD settings for APHYNITY.*

5 Related work

5.1 Hybrid modelling

Hybrid Learning, or gray box modelling as called in its early days in the 90’s (Psychogios & Ungar, 1992; Rico-Martinez et al., 1994; Thompson & Kramer, 1994; Rivera-Sampayo & Vélez-Reyes, 2001; Braun & Chaturvedi, 2002), has been a popular method to learn models that are both expressive and interpretable, while also allowing them to be learnt on fewer data. The interest for hybrid learning (Mehta et al., 2020; Lei & Mirams, 2021; Reichstein et al., 2019; Saha et al., 2020; Guen & Thome, 2020; Levine & Stuart, 2021; Espeholt et al., 2021) has greatly increased since the outbreak of recent neural network architectures that simplify the combination of physical equations within ML models. As an example, Neural ODEs (Chen et al., 2018) and convolutional neural networks (LeCun et al., 1995, CNN) are privileged architectures to work with dynamical systems described by ODEs or PDEs. While most of the literature focus on the predictive performance of hybrid models, recent work have also shown that this framework helps to infer the physical parameters accurately (Yin et al., 2021; Takeishi & Kalousis, 2021). This is aligned with Zyla et al. (2020) (see Section 4.0.2.2.2) which observe that inference on incomplete models results in a *systematic bias*. Similar to hybrid learning, they extend the model with *nuisance* parameters in order to improve its fidelity, and to reduce the systematic bias.

In this work, we decided to study Yin et al. (2021) and Takeishi & Kalousis (2021) for two reasons that distinguish them from the rest of the literature. First, these are notable examples of algorithms that can be applied to a broad class of problems in contrast to papers that focus on specific applications (Lei & Mirams, 2021; Reichstein et al., 2019). Second, those methods also learn a reliable inference model for the physical parameters, suggesting that the expert model is used properly in the generative model, which is a key assumption for our augmentation. While Takeishi & Kalousis (2021) claim to achieve robustness, we argue that this statement is incomplete as HVAE fails in OOD settings. In particular, their approach is only able to generalize with respect to unseen time or initial state if the model correctly identifies the latent variables z_a, z_e . HVAE cannot generalize to new physical parameters because the encoder’s validity is bound to the training set for the physical parameters.

5.2 Combining hybrid modelling and data augmentation

Close to our idea is the one proposed in Shrivastava et al. (2017) where they train a GAN model that improves the realism of a simulated image while conserving its semantic content (e.g., eyes colour) as modeled by the simulation parameters. The generated data with their annotations may then be used for a downstream task, such as inferring the properties of real images that corresponds to simulation parameters. The GAN objective from Shrivastava et al. (2017) requires that the two distributions induced by the semantic content of real and simulated data are identical. On the opposite, we consider training data that corresponds to expert parameters with limited diversity, and overcome this scarcity with expert augmentation. Another line of work similar to ours is Sim2Real, which considers the task of transferring a model trained on simulated data to real world (Doersch & Zisserman, 2019; Sadeghi et al., 2018; 2017). Robust hybrid learning, as a way to enhance simulations, could be used for Sim2Real.

5.3 Robust ML and invariant learning

Various statistical methods have been introduced to ensure models generalize under distribution shift. Domain-adversarial objectives aimed at learning (conditionally) invariant predictors (Ganin et al., 2016; Zhang et al., 2017; Li et al., 2018), GroupDRO (Sagawa et al., 2019) optimizing for worst-case loss over multiple domains and IRM (Arjovsky et al., 2019) as well as sub-group calibration (Wald et al., 2021) aiming to satisfy calibration or sufficiency constraints to learn features invariant across domains. Extensions, able to infer domain labels from training data have been proposed as well (Lahoti et al., 2020; Creager et al., 2021), partially inspired by fairness objectives (Hébert-Johnson et al., 2018; Kim et al., 2019). In contrast to AHM, all of these methods rely on the variation of interest being present in the training data.

6 Discussion

We now discuss the potential limitations of our method and its underlying assumptions.

Erroneous interaction model. The exactness of the hybrid component $p_\theta(y|x, y_e, z_a)$ is a critical assumption underlying our expert-based augmentation strategy. Unfortunately, this component is learned from training data only. Hence, we cannot prove its exactness on the test domain in the general case as the input domain over \mathcal{Y}_e may be different from the training. However, we argue that assumptions on the class of interaction model may alleviate this problem. As an example, we might consider to chose the best interaction model over a fixed set of potential interaction. If the correct interaction is present in this set we should eventually select it from data. A less extreme example is when we consider an additive hybrid model and embed this hypothesis into the interaction model, generalization to unseen y_e follows as long as the range of values is the same as in the training set. If this assumption is too strong, we could still expect that $p_\theta(y|x, y_e, z_a)$ generalizes to unseen y_e because hybrid learning drives y samples from p_θ to be close to y_e . It implies that the corresponding function approximator is stable, which helps generalizing to unseen scenarios. However, we must acknowledge that we cannot guarantee the stability of the interaction model in the general case. Thus, in practice, finding a good inductive bias for the interaction model may be important. However, we expect that in many cases it is easier to embed the right inductive bias in the interaction model rather than in the encoder. Indeed, the parameter identification (the encoder q_ψ) is often less-well understood or more complex than the generative model itself.

Diagnostic. While crucial, we cannot guarantee the exactness of the decoder p_θ in general because we only evaluate the encoder and the decoder jointly on data points (x, y, x_o, y_o) . However, in some cases we can detect model misspecification by observing that the predictive model $p_{\theta, \psi}(y|x, x_o, y_o)$ is imperfect. Making this observation is not always simple as it requires prior knowledge on the expected accuracy of an exact model. However, when the system is deterministically identifiable, we may argue that the accuracy should be only limited by the intrinsic noise between x and y given z_a and z_e .

Relaxing exactness. Even with a solid inductive bias on the decoder, achieving exactness is hard to achieve in practical settings. However, our experiments demonstrate that expert-augmentation works in practice. We can explain this by looking at Figure 3. If the generative model that maps x and (z_a, z_e) is incorrect, the mapping from \mathcal{Z}_a and \mathcal{Z}_e could be slightly off from Ω^+ . However, this does not preclude the set of augmented samples from being closer to Ω^+ than Ω and from inducing a better predictive model on Ω^+ than the original model trained only on Ω . Another argument is the effectiveness of data augmentation for training classical deep learning models, which works well even when some augmentations do not generate realistic samples.

Limitations. We have considered expert models that are parameterized by a small number of parameters and are covered densely via sampling. For higher dimensional parameter space the augmentation strategy might become inapplicable. Hence, a more ingenious sampling strategy, such as worst-case sampling, would be required. Another difficulty is choosing a plausible range of parameters that contains both the train and the test support; this will often need a human expert in the loop. If the chosen distribution does not cover some test configurations the robustness guarantees for these configurations collapse. On the opposite, a distribution that is too broad may also impact negatively the quality of the model. For instance, learning the right encoding behaviour for those unnecessary configurations requires representation capacity that is then unavailable for IID configurations. In this case the model might perform worse than before augmentation on the training distribution. Indeed, the experimental results have shown that the training error may slightly increase while the test error decreases.

In addition, we assume that the train distribution of z_a is representative of the test distribution. We empirically observed that a softer version of this assumption could be enough. However, performance will eventually decline as the support of the test distribution for z_a is far from the training domain. Finally, we have only validated our expert augmentation for amortized inference settings. Nevertheless, online inference algorithms, such as Markov-chain Monte Carlo, also require careful tuning of their hyperparameters (Campbell

et al., 2021) or learning distributions (Brofos et al., 2022) to work in practice and are eventually tied to the specific problem of interest. Thus, there might be opportunities to generalize our expert augmentation to non-amortized settings.

7 Conclusion

We have described hybrid learning with a probabilistic model in which one component of the latent process, denoted the expert model, is known. In this context, we have established that state-of-the-art algorithms are vulnerable to distribution shifts. Grounded in this formalisation, we have derived that expert augmentations induce robustness to OOD settings if the said algorithms behave as expected. We have shown on a set of synthetic settings and on a real-world system the favorable effect of expert augmentation on the OOD performance where standard hybrid learning algorithm fails. Finally, we have discussed how our assumptions transfer to real-world settings and have described potential shortcomings.

Our augmentation should benefit from future progress in hybrid learning as it shall apply to most hybrid modelling algorithms. Providing more substantial constraints on the targeted hybrid model is an essential direction for further improving the robustness of hybrid models. For instance, the minimal description length principle (Grünwald, 2007) could be an excellent resource for investigating the balance between the model’s capacity and robustness. In parallel, empirical and theoretical investigations of the learnt interaction model’s properties in various practical settings would unlock new understandings of the capabilities and limitations of hybrid learning algorithms. In the context of expert augmentation, it should enable to do more realistic assumptions for its applicability and to derive more precisely the expected robustness gain. Future work is also needed to show how hybrid learning and expert augmentation translate into performance gain over classical ML on challenging real-world applications.

References

- Aghili, F. Energetically consistent model of slipping and sticking frictional impacts in multibody systems. *Multibody System Dynamics*, 48(2):193–209, 2020.
- Arjovsky, M., Bottou, L., Gulrajani, I., and Lopez-Paz, D. Invariant risk minimization. *arXiv preprint arXiv:1907.02893*, 2019.
- Asseman, A., Kornuta, T., and Ozcan, A. Learning beyond simulated physics. In *Modeling and Decision-making in the Spatiotemporal Domain Workshop*, 2018. URL <https://openreview.net/pdf?id=HylajWsRF7>.
- Braun, J. E. and Chaturvedi, N. An inverse gray-box model for transient building load prediction. *HVAC&R Research*, 8(1):73–99, 2002.
- Brofos, J., Gabrié, M., Brubaker, M. A., and Lederman, R. R. Adaptation of the independent metropolis-hastings sampler with normalizing flow proposals. In *International Conference on Artificial Intelligence and Statistics*, pp. 5949–5986. PMLR, 2022.
- Campbell, A., Chen, W., Stimper, V., Hernandez-Lobato, J. M., and Zhang, Y. A gradient based strategy for hamiltonian monte carlo hyperparameter optimization. In *International Conference on Machine Learning*, pp. 1238–1248. PMLR, 2021.
- Chen, R. T., Rubanova, Y., Bettencourt, J., and Duvenaud, D. Neural ordinary differential equations. In *Proceedings of the 32nd International Conference on Neural Information Processing Systems*, pp. 6572–6583, 2018.
- Crabtree, V. P. and Smith, P. R. Physiological models of the human vasculature and photoplethysmography. *Electronic Systems and Control Division Research, Department of Electronic and Electrical Engineering, Loughborough University*, pp. 60–63, 2003.
- Cranmer, M., Greydanus, S., Hoyer, S., Battaglia, P., Spergel, D., and Ho, S. Lagrangian neural networks. *arXiv preprint arXiv:2003.04630*, 2020.

- Creager, E., Jacobsen, J.-H., and Zemel, R. Environment inference for invariant learning. In *International Conference on Machine Learning*, pp. 2189–2200. PMLR, 2021.
- Cubuk, E. D., Zoph, B., Mane, D., Vasudevan, V., and Le, Q. V. Autoaugment: Learning augmentation strategies from data. In *Proceedings of the IEEE/CVF Conference on Computer Vision and Pattern Recognition*, pp. 113–123, 2019.
- Doersch, C. and Zisserman, A. Sim2real transfer learning for 3d human pose estimation: motion to the rescue. *Advances in Neural Information Processing Systems*, 32:12949–12961, 2019.
- Espeholt, L., Agrawal, S., Sønderby, C., Kumar, M., Heek, J., Bromberg, C., Gazean, C., Hickey, J., Bell, A., and Kalchbrenner, N. Skillful twelve hour precipitation forecasts using large context neural networks. *arXiv preprint arXiv:2111.07470*, 2021.
- Ganin, Y., Ustinova, E., Ajakan, H., Germain, P., Larochelle, H., Laviolette, F., Marchand, M., and Lempitsky, V. Domain-adversarial training of neural networks. *The Journal of Machine Learning Research*, 17(1): 2096–2030, 2016.
- Geirhos, R., Jacobsen, J.-H., Michaelis, C., Zemel, R., Brendel, W., Bethge, M., and Wichmann, F. A. Shortcut learning in deep neural networks. *Nature Machine Intelligence*, 2(11):665–673, 2020.
- Grünwald, P. D. *The Minimum Description Length Principle*. MIT press, 2007.
- Guen, V. L. and Thome, N. Disentangling physical dynamics from unknown factors for unsupervised video prediction. In *Proceedings of the IEEE/CVF Conference on Computer Vision and Pattern Recognition*, pp. 11474–11484, 2020.
- Gulrajani, I. and Lopez-Paz, D. In search of lost domain generalization. *arXiv preprint arXiv:2007.01434*, 2020.
- Hébert-Johnson, U., Kim, M., Reingold, O., and Rothblum, G. Multicalibration: Calibration for the (computationally-identifiable) masses. In *International Conference on Machine Learning*, pp. 1939–1948. PMLR, 2018.
- Hodgkin, A. L. and Huxley, A. F. A quantitative description of membrane current and its application to conduction and excitation in nerve. *The Journal of Physiology*, 117(4):500–544, 1952.
- Keriven, N. and Peyré, G. Universal invariant and equivariant graph neural networks. *Advances in Neural Information Processing Systems*, 32:7092–7101, 2019.
- Kim, M. P., Ghorbani, A., and Zou, J. Multiaccuracy: Black-box post-processing for fairness in classification. In *Proceedings of the 2019 AAAI/ACM Conference on AI, Ethics, and Society*, pp. 247–254, 2019.
- Koh, P. W., Sagawa, S., Marklund, H., Xie, S. M., Zhang, M., Balsubramani, A., Hu, W., Yasunaga, M., Phillips, R. L., Gao, I., et al. Wilds: A benchmark of in-the-wild distribution shifts. In *International Conference on Machine Learning*, pp. 5637–5664. PMLR, 2021.
- Krueger, D., Caballero, E., Jacobsen, J.-H., Zhang, A., Binas, J., Zhang, D., Le Priol, R., and Courville, A. Out-of-distribution generalization via risk extrapolation (rex). In *International Conference on Machine Learning*, pp. 5815–5826. PMLR, 2021.
- Lahoti, P., Beutel, A., Chen, J., Lee, K., Prost, F., Thain, N., Wang, X., and Chi, E. H. Fairness without demographics through adversarially reweighted learning. *arXiv preprint arXiv:2006.13114*, 2020.
- LeCun, Y., Bengio, Y., et al. Convolutional networks for images, speech, and time series. *The Handbook of Brain Theory and Neural Networks*, 3361(10), 1995.
- Lei, C. L. and Mirams, G. R. Neural network differential equations for ion channel modelling. *Frontiers in Physiology*, pp. 1166, 2021.

- Levine, M. E. and Stuart, A. M. A framework for machine learning of model error in dynamical systems. *arXiv preprint arXiv:2107.06658*, 2021.
- Li, Y., Tian, X., Gong, M., Liu, Y., Liu, T., Zhang, K., and Tao, D. Deep domain generalization via conditional invariant adversarial networks. In *Proceedings of the European Conference on Computer Vision (ECCV)*, pp. 624–639, 2018.
- Mahmood, O., Mansimov, E., Bonneau, R., and Cho, K. Masked graph modeling for molecule generation. *Nature Communications*, 12(1):1–12, 2021.
- Mehta, V., Char, I., Neiswanger, W., Chung, Y., Nelson, A. O., Boyer, M. D., Kolemen, E., and Schneider, J. Neural dynamical systems: Balancing structure and flexibility in physical prediction. *arXiv preprint arXiv:2006.12682*, 2020.
- Psichogios, D. C. and Ungar, L. H. A hybrid neural network-first principles approach to process modeling. *AIChE Journal*, 38(10):1499–1511, 1992.
- Qian, Z., Zame, W. R., van der Schaar, M., Fleuren, L. M., and Elbers, P. Integrating expert odes into neural odes: Pharmacology and disease progression. *arXiv preprint arXiv:2106.02875*, 2021.
- Reichstein, M., Camps-Valls, G., Stevens, B., Jung, M., Denzler, J., Carvalhais, N., et al. Deep learning and process understanding for data-driven earth system science. *Nature*, 566(7743):195–204, 2019.
- Rico-Martinez, R., Anderson, J., and Kevrekidis, I. Continuous-time nonlinear signal processing: a neural network based approach for gray box identification. In *Proceedings of IEEE Workshop on Neural Networks for Signal Processing*, pp. 596–605. IEEE, 1994.
- Rivera-Sampayo, R. and Vélez-Reyes, M. Gray-box modeling of electric drive systems using neural networks. In *Proceedings of the 2001 IEEE International Conference on Control Applications (CCA '01)(Cat. No. 01CH37204)*, pp. 146–151. IEEE, 2001.
- Sadeghi, F., Toshev, A., Jang, E., and Levine, S. Sim2real view invariant visual servoing by recurrent control. *arXiv preprint arXiv:1712.07642*, 2017.
- Sadeghi, F., Toshev, A., Jang, E., and Levine, S. Sim2real viewpoint invariant visual servoing by recurrent control. In *Proceedings of the IEEE Conference on Computer Vision and Pattern Recognition*, pp. 4691–4699, 2018.
- Sagawa, S., Koh, P. W., Hashimoto, T. B., and Liang, P. Distributionally robust neural networks for group shifts: On the importance of regularization for worst-case generalization. In *International Conference on Learning Representations*, 2019.
- Saha, P., Dash, S., and Mukhopadhyay, S. Physics-incorporated convolutional recurrent neural networks for source identification and forecasting of dynamical systems. *arXiv preprint arXiv:2004.06243*, 2020.
- Shrivastava, A., Pfister, T., Tuzel, O., Susskind, J., Wang, W., and Webb, R. Learning from simulated and unsupervised images through adversarial training. In *Proceedings of the IEEE Conference on Computer Vision and Pattern Recognition*, pp. 2107–2116, 2017.
- Silver, D., Schrittwieser, J., Simonyan, K., Antonoglou, I., Huang, A., Guez, A., Hubert, T., Baker, L., Lai, M., Bolton, A., et al. Mastering the game of go without human knowledge. *Nature*, 550(7676):354–359, 2017.
- Stachowiak, T. and Okada, T. A numerical analysis of chaos in the double pendulum. *Chaos, Solitons & Fractals*, 29(2):417–422, 2006.
- Takeishi, N. and Kalousis, A. Physics-integrated variational autoencoders for robust and interpretable generative modeling. *Advances in Neural Information Processing Systems*, 34, 2021.

- Thompson, M. L. and Kramer, M. A. Modeling chemical processes using prior knowledge and neural networks. *AIChE Journal*, 40(8):1328–1340, 1994.
- Wald, Y., Feder, A., Greenfeld, D., and Shalit, U. On calibration and out-of-domain generalization. *arXiv preprint arXiv:2102.10395*, 2021.
- Xu, K., Hu, W., Leskovec, J., and Jegelka, S. How powerful are graph neural networks? *arXiv preprint arXiv:1810.00826*, 2018.
- Yin, Y., Le Guen, V., Dona, J., de Bézenac, E., Ayed, I., Thome, N., and Gallinari, P. Augmenting physical models with deep networks for complex dynamics forecasting. *Journal of Statistical Mechanics: Theory and Experiment*, 2021(12):124012, 2021.
- Zhang, Y., Barzilay, R., and Jaakkola, T. Aspect-augmented adversarial networks for domain adaptation. *Transactions of the Association for Computational Linguistics*, 5:515–528, 2017.
- Zyla, P. et al. Review of Particle Physics. *PTEP*, 2020(8):083C01, 2020. doi: 10.1093/ptep/ptaa104.

A Additional description of expert augmentation

We provide the procedure to do expert augmentation for robust hybrid learning as the sequence of steps below.

1. Train both the encoder $q_\psi(z_a, z_e|x, y)$ and the interaction model $p_\theta(y|x_o, z_a, y_e)$ with a hybrid learning algorithm, by minimizing the corresponding loss $\mathcal{L}(\psi, \theta) = \mathbb{E}_{\mathcal{D}} [\ell(x, y; \theta, \psi)]$ on the training set \mathcal{D} ;
2. Decide on an augmented distribution $p^+(z_e)$ for z_e that contains both train and test scenarios;
3. Reproduce the following steps to generate a dataset \mathcal{D}^+ of observations and expert variables $(x, y, z_e) \sim \mathbb{E}_{p(z_a)p(y_e|z_e, x, y)} [p(z_e)p(x)p_\theta(y|y_e, z_a, x)]$:
 - (a) Sample (x_o, y_o) from the data;
 - (b) Sample z_a from the posterior $q_\psi(z_a|x_o, y_o)$;
 - (c) Sample z_e from $p^+(z_e)$;
 - (d) Push forward x, z_a and z_e in the generative model as $y_e \sim p(y_e|x_o, z_e)$ and $y \sim p_\theta(y|x_o, z_a, y_e)$;
 - (e) Add the triplet (x_o, y, z_e) to the augmented training set \mathcal{D}^+ .
4. Freeze the interaction model, and fine-tune the encoder $q_\psi(z_a, z_e|x, y)$ on the augmented dataset \mathcal{D}^+ by minimizing $\mathcal{L}^+(\psi, \theta) = \mathbb{E}_{\mathcal{D}^+} [\ell(x, y; \theta, \psi) - \log q_\psi(z_e|x, y)]$.

Algorithm 2 Expert augmented hybrid learning

```

1:  $\mathcal{D} := \{(x^{(i)}, y^{(i)})\}_{i=1}^N \in (\mathcal{X} \times \mathcal{Y})^N$  ▷ A training set
2:  $q_\psi(z_a, z_e|x, y)$  ▷ A parametric encoder
3:  $p(y_e|x, z_e)$  ▷ An expert model
4:  $p_\theta(y|x, y_e, z_a)$  ▷ A parametric decoder
5:  $l(x, y, \theta, \psi)$  ▷ A hybrid learning objective function
6:  $p_+(z_e)$  ▷ A prior distribution on  $z_e$  that covers both train and test scenarios
7: procedure TRAINING
8:    $\psi^*, \theta^* \leftarrow \arg \min_{\psi, \theta} \mathbb{E}_{(x, y) \sim \mathcal{D}} [l(x, y, \theta, \psi)]$ 
9:    $\mathcal{D}^+ \leftarrow \text{GENERATEAUGMENTEDSET}$ 
10:   $\psi^* \leftarrow \arg \min_{\psi} \mathbb{E}_{(x, y, z_e) \sim \mathcal{D}^+} [l(x, y, \theta^*, \psi) - \log q_\psi(z_e|x, y)]$ 
11:  return  $\psi^*, \theta^*$ 
12: end procedure
13: procedure GENERATEAUGMENTEDSET
14:   $\mathcal{D}^+ \leftarrow \{\}$ 
15:  for each  $(x_o, y_o) \in \mathcal{D}$  do
16:     $z_a \sim q_{\psi^*}(z_a, z_e|x_o, y_o)$ 
17:     $z_e \sim p_+(z_e)$ 
18:     $y_e \sim p(y_e|x_o, z_e)$ 
19:     $y \sim p_{\theta^*}(y|x_o, y_e, z_a)$ 
20:     $\mathcal{D}^+ \leftarrow \mathcal{D}^+ \cup \{(x_o, y, z_e)\}$ 
21:  end for
22:  return  $\mathcal{D}^+$ 
23: end procedure

```

B Additional details on the hybrid-VAE

We now provide the definition of the different regularizers employed by the hybrid-VAE. Our definition slightly differs from Takeishi & Kalousis (2021) as we explicitly accounts for known input variables x and

thus consider a dataset of pairs (x, y) . Although our framework should hold for non-deterministic expert models, we have directly employed the regularizers proposed by Takeishi & Kalousis (2021) which assume a deterministic expert models. We encourage the non-familiar reader to check the original work on hybrid-VAE for a thorough discussion of the effect of the different regularizers.

The first regularizer R_{PPC} aims to inhibit unnecessary flexibility of the learned parts of the decoder. To this purpose, Takeishi & Kalousis (2021) proposes to minimize the Kullback-Leibler divergence between the posterior predictive distributions of the hybrid model and the expert model:

$$\mathbb{KL} [p_{\theta, \psi}(y|\mathcal{D}) || p_{\theta, \psi}^e(y|\mathcal{D})],$$

where

$$p_{\theta, \psi}(y|\mathcal{D}) = \int p_{\theta}(y|x_o, z_a, z_e) q_{\psi}(z_a, z_e|x_o, y_o) p_{\mathcal{D}}(x_o, y_o) dx_o dy_o dz_a dz_e,$$

and

$$p_{\theta, \psi}^e(y|\mathcal{D}) = \int p_{\theta}(y_e|x_o, z_e) q_{\psi}(z_e|x_o, y_o) p_{\mathcal{D}}(x_o, y_o) dx_o dy_o dz_e.$$

As the posterior predictive distributions are intractable, Takeishi & Kalousis (2021) introduce a lower bound on it as

$$R_{PPC} = \mathbb{E}_{x_o, x_e, y_o \sim p_{\mathcal{D}}} [\mathbb{E}_{q(z_a, z_e|x_o, y_o)} \mathbb{KL} [p_{\theta}(y|x, z_a, z_e) || p_{\theta}(y_e|x, z_e)] + \mathbb{KL} [q_{\psi}(z_a, z_e|x_o, y_o) || p(z_a)p(z_e)]] .$$

The second regularizer $R_{DA,1}$ helps the two-steps encoder of the hybrid-vae to be grounded into the physics. The first encoder should map the input to signals that can be produced by the expert model. Formally, Takeishi & Kalousis (2021) propose to enforce this with

$$R_{DA,1} = \mathbb{E}_{p_{\mathcal{D}}(x_o, x_e, y_o) q(z_a|x_o, y_o)} [||g_{P,1}(x_o, y_o, z_a) - \text{sg}(y_e(x_o, z_e = g_{P,2}(g_{P,1}(x_o, y_o, z_a))))||_2^2],$$

where the encoder first output a posterior $q(z_a|x_o, y_o)$ for z_a , then transform y_o into something that should match the expert model with $g_{P,1}$, and finally $g_{P,2}$ output the posterior distribution over the physical parameters. The symbol sg denote the stop gradient operator.

Finally, the third regularizer helps the second second step of encoding $g_{P,2}$ to properly encode any physical configuration. In particular, it should be able to encode properly any pair (x, y_e) that we could generate with the expert model. The regularizer takes the form

$$R_{DA,2} = \mathbb{E}_{x, z_e} ||g_{P,2}(y_e(x, z_e)) - z_e||_2^2.$$

C Additional details on experiments

C.1 Hyperparameter Search

For the three synthetic experiments with APHYNITY, we have performed a bayesian optimization search with 4×100 trials to find this set of hyperparameters. The ranges for the search were: $\tau_2 \in [0, 10]$, $\lambda_0 \in [0, 20]$, weight decay $\in [0, 0.1]$, $N_{iter} \in \{0, \dots, 10\}$, $\text{lr} \in [0.0005, 0.1]$.

For the three synthetic experiments with HVAE, we have performed a bayesian optimization search with 20×25 trials to find this set of hyperparameters. The ranges for the search were: $\alpha \in [0, 100]$, $\beta \in [0, 100]$, $\gamma \in [0, 100]$, $\text{lr} \in \{0.001, 0.0005, 0.0001\}$.

From the result of these searches we have chosen the hyperparameters values provided below. Reproducing our experiments by re-generating new synthetic datasets can change the numbers. However we have observed a constant benefit of applying the expert augmentation even when the non-augmented model was not tuned perfectly.

For the double pendulum experiment we did not run any hyperparameter search and there might exist better set of hyperparameters. However, our objective was only to show that expert augmentation helps to gain

performance in OOD settings, even when the experiments is not well-controlled. We believe our conclusion should not be sensitive to applying augmentation on a better fine-tuned model. Our theory suggest the opposite: if the model is better, it should be able to generate good augmented samples and gain generalization capabilities.

C.2 Damped pendulum

Datasets. We use Neural Ordinary Differential Equations (NODE) (Chen et al., 2018) to solve the ODE ruling the damped pendulum. Each sample is simulated for $t_0 = 0s$, $t_1 = 5s$, and $t_2 = 20s$, with a time resolution equal to 0.1 second. The models are trained with only the realizations between t_0 and t_1 . At test and validation time, the pair $(x_o, y_o) = (y_0, [y_{i\Delta t}]_{i=1}^{t_1/\Delta t})$, $x = y_{t_1}$ and the model predicts $y = [y_{i\Delta t}]_{i=t_2/\Delta t+1}^{t_2/\Delta t}$. The initial angular speed is always 0 and $\theta_0 \sim \mathcal{U}(-\frac{\pi}{2}, \frac{\pi}{2})$.

The training set is made of 1000 samples and the validation set of 100 samples. They are both generated by sampling uniformly $z_a := \alpha$ from $\mathcal{Z}_a := [0, 0.6]$ and $z_e := \omega_0$ from $\mathcal{Z}_e := [1.5, 3.1]$. The shifted test set contains 100 samples generated by sampling uniformly z_a in \mathcal{Z}_a and z_e in $\tilde{\mathcal{Z}}_e := [0.5, 1.5]$.

APHYNITY. Our model is composed of a 1-layer RNN with 128 units that encodes the input signal $y_{0:t_1}$ as $h(y_{0:t_1}) \in \mathbb{R}^{128}$. An MLP with 3 layers of 150 units and ReLU activations maps h to \mathbb{R}_+ to predict ω_0 . The function $f_a : \mathbb{R}^{128} \times \mathbb{R}^2$ is an MLP with 3 layers of 50 units and ReLU activations (no activation for the last layer). The models are trained for 50 epochs with Adam with no weight decay and a learning rate equal to 0.0005. For the Lagrangian optimization we use $N_{iter} = 5$, $\lambda_0 = 10$, $\tau_2 = 5$ (see (Yin et al., 2021)). The augmented data are generated by sampling uniformly $z_e \in \tilde{\mathcal{Z}}_e^+ := [0.5, 3.5]$ and z_a from the marginal predictive prediction of the model, that is we use the training dataset to infer values of z_a and use these as samples. The batch size is 100.

HVAE. We use the notations from Takeishi & Kalousis (2021) to describe the architecture of the VAE. The network $g_{p,1} : \mathbb{R}^2 \times \mathbb{R}^{d_a}$, where $d_a = 1$ is the size of the latent space for the interaction model, is supposed to filter the observations so that they can be generated by the expert model. It has 2 hidden layers with 128 units, $g_{p,2}$ is an MLP with the following hidden layers [128, 128, 256, 64, 32] and takes the full sequence of filtered states and predicts the mean and variance of a normal distribution that parameterize the posterior $p_\theta(z_e|x, y, z_a)$. Another network, g_a takes the sequence of observations and predict the posterior distribution of z_a as a normal distribution. This network has the following hidden layers [256, 256, 128, 32]. All networks have SeLU activations. In general the decoder of HVAE can be anything that combines the expert model in order to produce samples in the observation space, as we made the hypothesis that the ODE is just missing an additive term, the decoder is a NODE where the function is the sum of f_e and f_a a two hidden layers MLP with 64 units and SeLU activation (except for the last layer that has no activation). The likelihood model is also Gaussian with the mean being predicted by the NODE and the variance learned but shared for all observations. For additional details on our architecture and implementation details we encourage the interested reader to check our code.

The networks are trained jointly for 1000 epochs with Adam optimizer, with a learning rate equal to 0.0005, weight decay equal to 0.000001 and batch size 200. The other parameters are set to $\gamma = 1$, $\alpha = 0.01$ and $\beta = 0.01$. The HVAE also relies on some augmentation during training and in order to compare fairly our model to theirs we use the same distribution for our augmentation and theirs that is $z_a \sim \mathcal{N}(0, I)$ and $z_e \sim \mathcal{U}(0.5, 3.5)$.

C.3 RLC series

Datasets. Similar to the damped pendulum, we use NODE to solve the ODE ruling the RLC circuit. Each sample is simulated for $t_0 = 0s$, $t_1 = 5s$, and $t_2 = 20s$, with a time resolution equal to 0.1 second. The models are trained with only the realizations between t_0 and t_1 . At test and validation time, the pair $(x_o, y_o) = (y_0, [y_{i\Delta t}]_{i=1}^{t_1/\Delta t})$, $x = y_{t_1}$ and the model predicts $y = [y_{i\Delta t}]_{i=t_2/\Delta t+1}^{t_2/\Delta t}$. In all experiments, the initial value for $U_0 \sim \mathcal{N}(0, 1)$ and $I_0 = 0$, the voltage source delivers a AC + DC tension $V(t) = 2.5 \sin(4\pi t) + 1$.

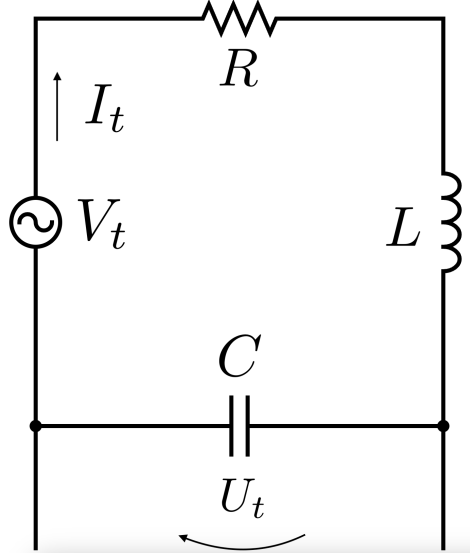


Figure 10: A generic schematic of a RLC series circuit.

The training set is made of 2000 samples and the validation set of 100 samples. They are both generated by sampling uniformly $z_a := R$ from $\mathcal{Z}_a := [1, 3]$ and $z_e := [L, C]$ from $\mathcal{Z}_e := [1, 3] \times [0.5, 1.5]$. The shifted test set contains 100 samples and is generated by sampling uniformly z_a in \mathcal{Z}_a and z_e in $\tilde{\mathcal{Z}}_e := [3, 5] \times [1., 2.5]$.

APHYNITY. Our model is composed of a 1-layer RNN with 128 units that encodes the input signal $y_{0:t_1}$ as $h(y_{0:t_1}) \in \mathbb{R}^{128}$. An MLP with 3 layers of 200 units and ReLU activations maps h to \mathbb{R}_+^2 that predicts L and C . The function $f_a : \mathbb{R}^{128} \times \mathbb{R}^2$ is an MLP with 3 layers of 150 units and ReLU activations (no activation for the last layer). The models are trained for 50 epochs with Adam with no weight decay and a learning rate equal to 0.0005. For the Lagrangian optimization we use $N_{iter} = 5$, $\lambda_0 = 10$, $\tau_2 = 5$ (see (Yin et al., 2021)). The augmented data are generated by sampling uniformly $z_e \in \tilde{\mathcal{Z}}_e^+ := [1, 5] \times [0.5, 2.5]$ and z_a from the marginal predictive prediction of the model, that is we use the training dataset to infer values of z_a and use these as samples. The batch size is 100.

HVAE. We use the same networks' architectures than for the damped pendulum experiment. Except that $g_{p,1}$ is has 3 hidden layers with 100 units.

The networks are trained jointly for 1000 epochs with Adam optimizer, with a learning rate equal to 0.0005, weight decay equal to 0.000001 and batch size 100. The other parameters are set to $\gamma = 1$, $\alpha = 0.01$ and $\beta = 0.01$. The HVAE also relies on some augmentation during training and in order to compare fairly our model to theirs we use the same distribution for our augmentation and theirs that is $z_a \sim \mathcal{N}(0, I)$ and $z_e \sim \mathcal{U}(1, 5) \times \mathcal{U}(0.5, 2.5)$.

C.4 2D reaction diffusion

Datasets. Similar to the damped pendulum, we use NODE to solve the PDE ruling the reaction diffusion. We closely follow the experimental setting described in Yin et al. (2021) and approximate the Laplace operator with a 3×3 discrete version of the operator. Each sample is simulated for $t_0 = 0s$, $t_1 = 1s$, and $t_2 = 5s$, with a time resolution equal to 0.1 second. The models are trained with only the realizations between t_0

and t_1 . At test and validation time, the pair $(x_o, y_o) = (y_0, [y_{i\Delta t}]_{i=1}^{t_1/\Delta t})$, $x = y_{t_1}$ and the model predicts $y = [y_{i\Delta t}]_{i=t_2/\Delta t+1}^{t_2/\Delta t}$. The initial state is sampled from a uniform distribution in $[0, 1]$.

The training set is made of 2000 samples and the validation set of 100 samples. They are both generated by sampling uniformly $z_a := k$ from $\mathcal{Z}_a := [0.003, 0.005]$ and $z_e := [a, b]$ from $\mathcal{Z}_e := [0.001, 0.002] \times [0.003, 0.007]$. The shifted test set contains 100 samples and is generated by sampling uniformly z_a in \mathcal{Z}_a and z_e in $\tilde{\mathcal{Z}}_e := [0.002, 0.004] \times [0.001, 0.1]$.

APHYNITY. Our model is composed of a deep CNN that encodes the input sequence of 10 images. The exact architecture can be found in the code. The dimension of z_a is equal to 10. Similarly to Yin et al. (2021) the function f_a is a 3-layers CNN with ReLU activations. The models are trained for 500 epochs with Adam with no weight decay and a learning rate equal to 0.0005. For the Lagrangian optimization we use $N_{iter} = 1, \lambda_0 = 10, \tau_2 = 5$. The augmented data are generated by sampling uniformly $z_e \in \mathcal{Z}_e^+ := [0.001, 0.004] \times [0.001, 0.01]$ and z_a from the marginal predictive prediction of the model, that is we use the training dataset to infer values of z_a and use these as samples. The batch size is 100.

C.4.1 HVAE

We use the notations from Takeishi & Kalousis (2021) to describe the architecture of the VAE. The network $g_{p,1} : \mathbb{R}^{2 \times 32 \times 32} \times \mathbb{R}^{d_a}$ is a conditional U-net, where $d_a = 10$ is the size of the latent space for the interaction model, is supposed to filter the observation so that they can be generated by the expert model. The networks $g_{p,1}$ and g_a share a common backbone CNN and are, in addition, respectively parameterized by 2 3-layers MLPs. All networks have ReLU activations. In general the decoder of HVAE can be anything that combines the expert model in order to produce samples in the observation space, as we made the hypothesis that the ODE is just missing an additive term, the decoder is a NODE where the function is the sum of f_e and f_a a 3-layers CNN. The likelihood model is also Gaussian with the mean being predicted by the NODE and the variance learned but shared for all observations. For additional details on our architecture and implementation details we encourage the interested reader to check our code.

The networks are trained jointly for 1000 epochs with Adam optimizer, with a learning rate equal to 0.0005, weight decay equal to 0.00001 and batch size 100. The other parameters are set to $\gamma = 1, \alpha = 0.01$ and $\beta = 0.01$. The HVAE also relies on some augmentation during training and in order to compare fairly our model to theirs we use the same distribution for our augmentation and theirs that is $z_a \sim \mathcal{N}(0, I)$ and $z_e \sim \mathcal{U}(0.001, 0.004) \times \mathcal{U}(0.001, 0.01)$.

C.5 Double pendulum

Figure 11 shows the marginal distributions of the angular positions and speeds in the artificially split training, validation and testing sets. We use this plot to inform the bounds of the uniform distributions we use to do the expert augmentation.

In this experiment, we only used APHYNITY because our main goal was just to show the effectiveness of the augmented version and not to compare HVAE to APHYNITY. In order to make APHYNITY works, we had to extensively search for good hyperparameters. We eventually reach the following setup. The encoder is a fully connected neural network with 3 layers of 300 neurons. F_a is also a fully connected neural network with 3 layers of 300 neurons and $z_a \in \mathbb{R}^{10}$. The models are trained for 100 epochs with Adam with no weight decay and a learning rate equal to 0.0005. For the Lagrangian optimization we use $N_{iter} = 1, \lambda_0 = 1000, \tau_2 = 5$. The batch size is 100.

The augmented data are generated by sampling uniformly $z_e \in \mathcal{Z}_e^+ := [-15, 15] \times [-30, 30]$ and z_a from the marginal predictive prediction of the model, that is we use the training dataset to infer values of z_a and use these as samples. These bounds were chosen by looking at the distribution in Figure 11.

D Supplementary results

We now provide additional results for AHM versus standard models.

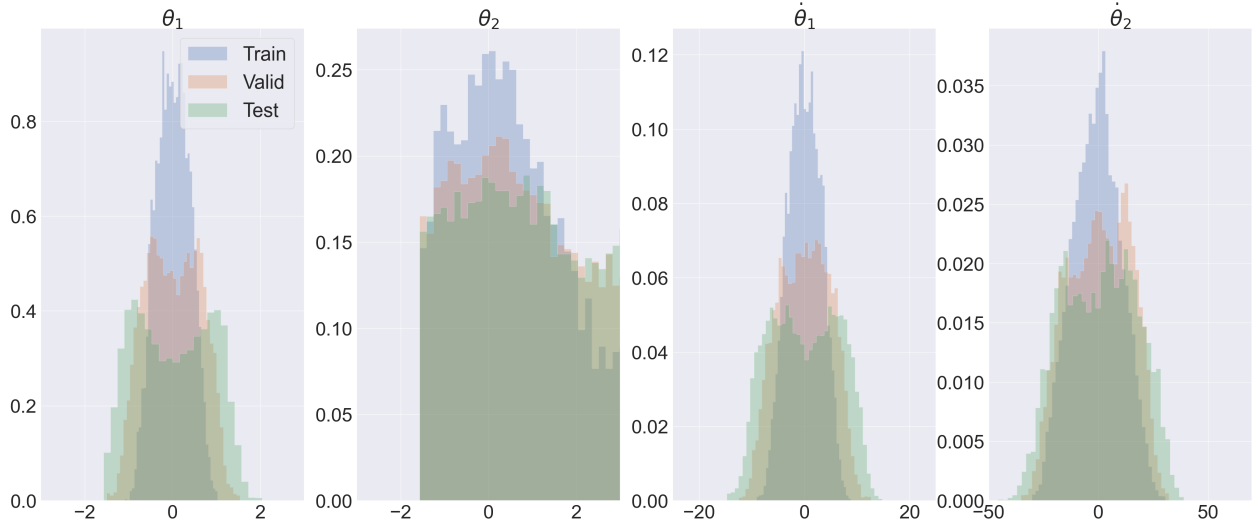


Figure 11: The distributions of initial angular positions and speeds in the experiment of the double pendulum.

D.1 Log-mses on the three synthetic problems

Table 1 presents the log-mses numbers on the three synthetic problems.

Dataset		APH.	HVAE	APH.+	HVAE+
Pendulum	Val.	-2.7 ± 0.3	-2.9 ± 0.5	-3.4 ± 0.3	-2.9 ± 0.6
	Test	-0.9 ± 0.2	-1.2 ± 0.2	-3.3 ± 0.3	-3.1 ± 0.3
RLC	Val.	-6.3 ± 0.2	-4.3 ± 0.1	-6.8 ± 0.2	-3.8 ± 1.5
	Test	-2.5 ± 0.1	-2.2 ± 0.1	-3.0 ± 0.3	-2.1 ± 0.3
Diffusion	Val.	-2.9 ± 0.3	-3.4 ± 0.2	-2.7 ± 0.3	-3.3 ± 0.3
	Test	1.0 ± 0.4	0.9 ± 0.8	-2.9 ± 0.2	-3.5 ± 0.1

Table 1: Comparison of the log-mse of different hybrid modelling strategies in validation and OOD test settings. *Except on RLC, AHMs always outperform the corresponding hybrid learning models on the test sets. Good performance on the validation set are conserved with augmentation.*

D.2 Distribution shift visualization

Similar to Figure 1, Figure 12 and Figure 13 showcase the behaviour of APHYNITY and APHYNITY+ for OOD test samples.

D.3 On the effect of out of expertise shift

The additional results in Figure 14, Figure 15 and Figure 16 demonstrate that our augmentations is mostly always beneficial. Although the benefit of augmentation decreases with the gap between the support of the distributions of z_a and train and test times, it still performs either better or on par with non-augmented hybrid learning models.

D.4 Applying augmentation at multiple stage of the learning

In order to check the robustness of applying the expert augmentation in practical settings, for the quality of the interaction model is unknown, we study the improvement brought by applying augmentation at the different stage of the training. Figure 17 shows that our augmentation robustly improves the test performance, even when the finetuning is performed on models that are not trained until convergence. We also observe

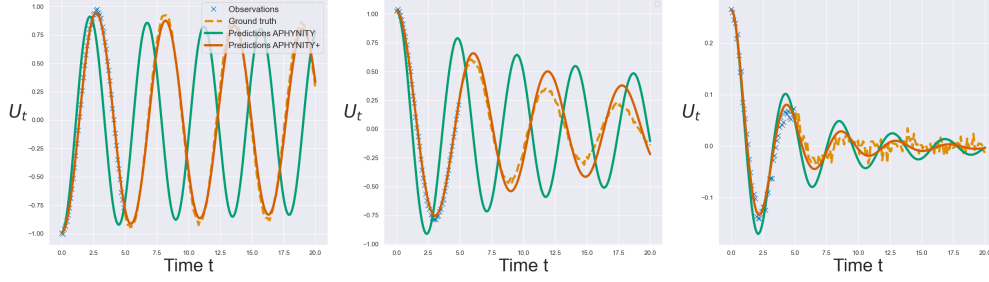


Figure 12: Comparison of the predictions made by APHYNITY and APHYNITY+ on the damped pendulum problem for 3 diverse test examples. It is important to mention that the support of the test distribution is disjoint from the training support. *We clearly observe the beneficial effect of augmentation which lead to more accurate predictions.*

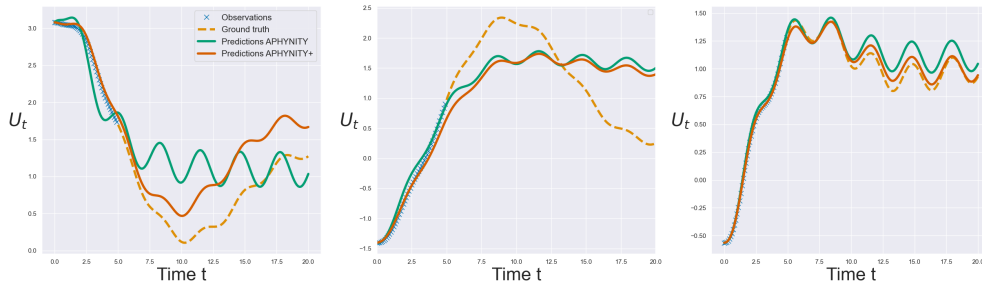


Figure 13: Comparison of the predictions made by APHYNITY and APHYNITY+ on the RLC series problem for 3 diverse test examples. It is important to mention that the support of the test distribution is disjoint from the training support. *We can perceive the beneficial effect of augmentation which lead to more accurate predictions in some cases. However both models are inaccurate. This indicates that the RLC series parameters are not easily identifiable, hence the generative model is not exact and augmentation is not as useful as for the diffusion and the pendulum.*

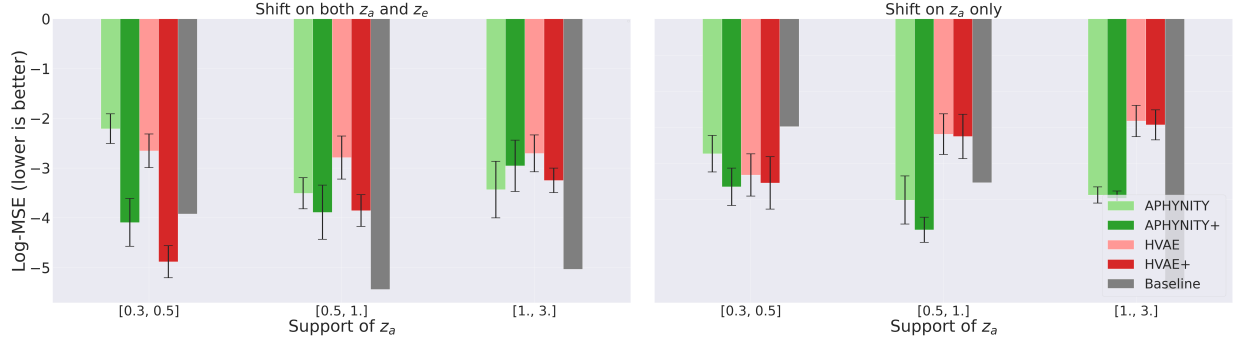


Figure 14: **Damped pendulum.** Effect of a distribution shift on the latent variable z_a of the interaction model. When the shift of z_a is reasonable (less than 1), the augmented models outperforms standard models even when the shift is only on z_a .

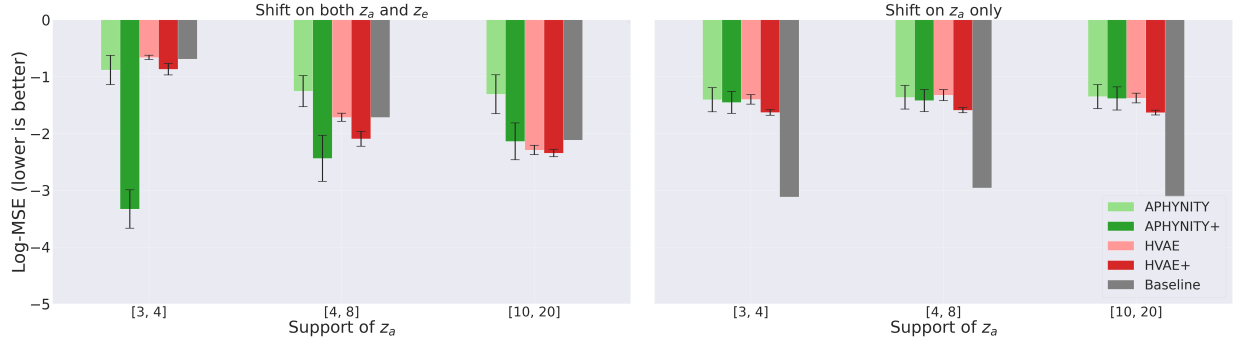


Figure 15: **RLC series.** Effect of a distribution shift on the latent variable z_a of the interaction model. We observe that augmentation is always beneficial, even when the shift is only on z_a . As the dynamics of the RLC series systems depends on the values of all 3 parameters R, L, C , we observe that some distribution shift can even lead to improved performance for the augmented models as for APHYNITY+ when $R \in [3, 4]$

that, as the model gets better trained, it takes more finetuning iterations to maintain the same validation performance. It is why in the results presented in the main text we used 100 epochs of finetuning in order to get the best improvements from the expert augmentation.

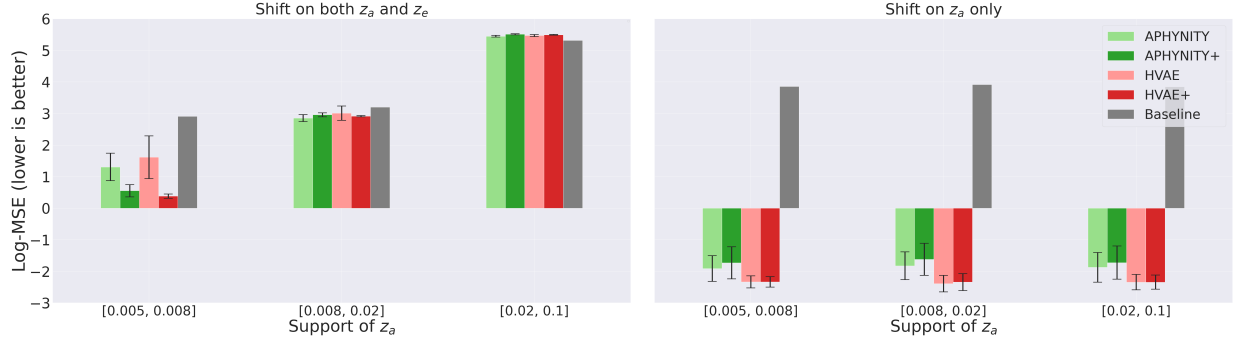


Figure 16: **2D diffusion reaction.** Effect of a distribution shift on the latent variable z_a of the interaction model. When the shift of z_a is reasonable ($k < 0.008$), the augmented models outperforms standard hybrid learning even when the shift is only on z_a .

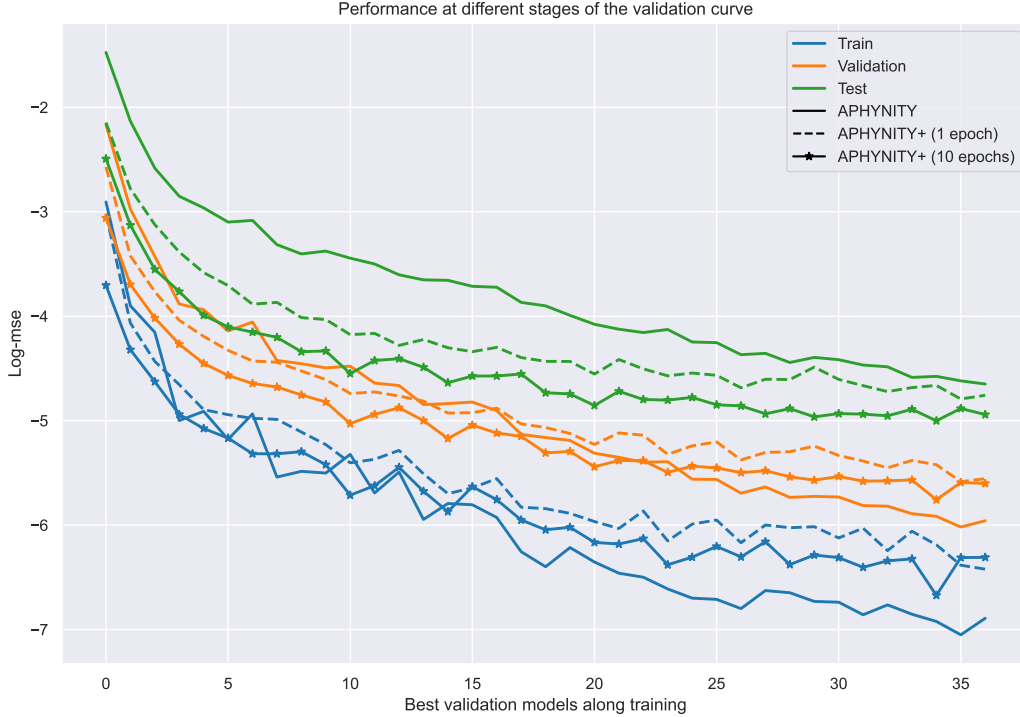


Figure 17: The performance of APHYNITY and APHYNITY+ along training. Plain lines represent the evolution of training, validation and test log-mse of APHYNITY on the double pendulum along training. Dashed lines and starred lines respectively depicts the performance when the corresponding model finetuned respectively for one and ten epochs. *Expert augmentation reduces the gap between the train, validation and test log-mses at any stage of the training. In particular it tends to slightly decrease the test performance and to improve the test performance, as expected from the augmentation strategy.*

E Optimal Bayes predictor

We define the optimal Bayes predictor from a family of approximators \mathcal{F} of a quantity y given an input x as the posterior distribution $q(y|x)$ that has a minimal error on the true posterior $p(x|y)$. We consider the Kullback-Leibler divergence as the objective and formally define the optimal Bayes predictor $p_B(y|x) \in \mathcal{F}$ as

$$p_B(y|x) = \arg \min_{q \in \mathcal{F}} \mathbb{E}_{p(y|x)} \left[\log \frac{p(y|x)}{q(y|x)} \right].$$

We assume the model in Figure 2 and are aiming for the Bayes optimal predictor of y given an input x and a pair of observations $p(x_o, y_o)$ taken from the same system; that is for $y \sim p(Y|x, z_a, z_e)$ and $y_o \sim p(Y|x_o, z_a, z_e)$ coming from the same system's parameters z_a and z_e but potentially different perturbations x (and x_o). We consider a class of predictors expressed as an expectation of a universal conditional distribution $q(z_a, z_e|(x_o, y_o))$ over a universal conditional distribution $q(y|x, z_a, z_e)$. Any elements in \mathcal{F} is defined as $\mathbb{E}_{q(z_a, z_e|(x_o, y_o))} [q(y|x, z_a, z_e)]$ where $q(z_a, z_e|(x_o, y_o))$ and $q(y|x, z_a, z_e)$ can be any continuous conditional distribution. We also consider that all quantities discussed belong to \mathbb{R}^k for $k \in \mathbb{N}$ and have continuous support. We aim to prove that $q(z_a, z_e|(x_o, y_o)) = p(z_a, z_e|(x_o, y_o))$ and $q(y|x, z_a, z_e) = p(y|x, z_a, z_e)$ constitutes the Bayes optimal predictor of y given (x, x_o, y_o) in \mathcal{F} . Indeed, we have:

$$\mathbb{E}_{p(z_a, z_e|(x_o, y_o))} [p(y|x, z_a, z_e)] = \int p(z_a, z_e|(x_o, y_o)) p(y|x, z_a, z_e) dz_a dz_e \quad (13)$$

$$= \int p(z_a, z_e|(x_o, y_o)) p(y|x, z_a, z_e, (x_o, y_o)) dz_a dz_e \quad (14)$$

$$= \int p(y, z_a, z_e|x, (x_o, y_o)) dz_a dz_e \quad (15)$$

$$= p(y|x, (x_o, y_o)), \quad (16)$$

and thus

$$\mathbb{KL} [p(y|x, x_o, y_o) || \mathbb{E}_{p(z_a, z_e|(x_o, y_o))} [p(y|x, z_a, z_e)]] = \mathbb{KL} [p(y|x, x_o, y_o) || p(y|x, (x_o, y_o))] = 0 \quad (17)$$

which is the minimal value of the objective function and is thus optimal.